Effects of alloying and hydrostatic pressure on electronic and optical properties of GaAs-$Al_xGa_{1-x}As$ superlattices and multiple-quantum-well structures

M. A. Gell,* D. Ninno, and M. Jaros
Department of Theoretical Physics, The University of Newcastle upon Tyne, Newcastle upon Tyne NE1 7RU, England, United Kingdom

D. J. Wolford, T. F. Keuch, and J. A. Bradley
IBM Thomas J. Watson Research Center, P.O. Box 218, Yorktown Heights, New York 10598
(Received 19 June 1986)

We have used our pseudopotential scheme to calculate electronic and optical properties of GaAs-$Al_xGa_{1-x}As$ superlattices and multiple-quantum-well structures as a function of alloying ($0 \leq x \leq 1$), hydrostatic pressure (0—50 kbar), and band offsets. We have obtained a full description of the electronic states both near the band edges and well into the range of energies above the confining barriers. In particular, we have shown how alloying can be used to mix Γ-like states with X-like states. Such mixing can lead to dramatic changes in the rapidly varying parts of the superlattice wave functions and alter appreciably the observable optical properties associated with such states. We also show that similar effects can be produced by the application of hydrostatic pressure. The electronic structure and optical properties of periodic structures with GaAs layers of width up to 102 Å and $Al_xGa_{1-x}As$ layers of width up to 514 Å have been studied. We show how mixing in wave-vector space between confined states and between confined states and extended bulk Bloch states leads to changes in observable properties, some of which can be exploited in order to determine band offsets. A representative set of data on the pressure dependence of optical spectra is used to make a comparison between theoretical and experimental results.

I. INTRODUCTION

Semiconductor superlattices are periodic structures consisting of at least two semiconductors, e.g., GaAs and $Al_xGa_{1-x}As$, arranged in alternating layers. The periodic spatial modulation results in a system which has a low effective dimensionality and, as a result, electronic and optical properties which are different from those associated with bulk crystals. It has been shown that the electronic states confined in GaAs by "barrier" layers of direct ($x \lesssim 0.35$) $Al_xGa_{1-x}As$, which is well lattice-matched to GaAs, can be modeled in terms of effective potentials which are microscopically smooth and which originate from spatially dependent zone-center band edges.[1,2] More detailed calculations have confirmed that the predictions of the particle-in-a-box model are basically correct.[3] However, a complete picture of the electronic structure in the energy range above the confining (Γ_6^c) barrier cannot be obtained within such a framework because the rapidly varying Bloch component of the total (superlattice) wave function and its changes at the interfaces are totally ignored. Such an assumption cannot be justified for cases in which $Al_xGa_{1-x}As$ is indirect or for cases in which the confined states are dominated by secondary-conduction-band minima lying close to the X and L points of the bulk Brillouin zone.

Until the formulation of our pseudopotential method, no scheme was able to give a complete[4] and accurate[5] description of the electronic and optical properties of superlattices in all interesting ranges of energy. Even the most accomplished methods based on the tight-binding formalism[6,7] include only nearest-neighbor parameters and consequently misrepresent the symmetry properties of states associated with secondary-conduction-band valleys. Our pseudopotential method is particularly useful for modeling structures in which crossing occurs between states derived from the center (Γ) and edges (X) of the bulk Brillouin zone. Such crossings may occur as a result of changes in alloy composition or changes in the widths of the layers[8] or may be induced by the application of hydrostatic pressure. Accordingly, we have made parallel theoretical and experimental studies of structures whose electronic structure is dominated by mixing between zone-center- and zone-edge-related states. In our first report,[9] in which experimental methods and results were emphasized, we presented pressure-dependent optical spectra for several multiquantum well structures. In particular, we showed that high-pressure techniques can be used to give a direct optical determination of band offsets in the GaAs-$Al_xGa_{1-x}As$ system. The present study is a complementary report in which theory is emphasized, although we make a direct comparison with representative experimental results in order to illustrate the way in which our predictions can be used in order to interpret experimental data. We hope in this study to provide a conceptual and factual basis for a more wide-ranging and comprehensive comparison between experimental and theoretical results which we intend to provide in our future publications.

II. METHOD

The direct lattices of GaAs and AlAs have the zinc-blende structure which may be considered as two face-centered cubic (fcc) structures displaced from each other by one-quarter of a body diagonal. The T_d symmetry associated with these bulk crystals is lowered when a superlattice is formed by alternating layers of, say, GaAs with layers of, say, AlAs in a particular direction. For example, the $(GaAs)_u(AlAs)_v$ (001) superlattice formed by alternating in the [001] direction u monolayers of GaAs with v monolayers of AlAs has the simple tetragonal structure with space-group symmetry D_{2d}^1 ($P\bar{4}2m$) for the case of even $(u+v)$ and space-group symmetry D_{2d}^{11} ($I\bar{4}2m$) for the case of odd $(u+v)$. In this paper, we define a monolayer to comprise one layer of anions plus one layer of cations and so the width of such a monolayer in the [001] direction is $A/2$, where A is the bulk lattice constant. We shall also restrict ourselves to the case of superlattices with even $(u+v)$ and so to superlattices with period $D=A(u+v)/2$.

The conventional unit cell of the fcc lattice has to be enlarged in the direction parallel with the superlattice axis in order to include one complete layer of GaAs and one complete layer of AlAs. This enlarged unit cell is then repeated indefinitely in all directions in order to form the complete (infinite) superlattice crystal. In Fig. 1(a) we show a set of primitive translation vectors $\mathbf{a}'$ for the fcc lattice and a set of primitive translation vectors $\mathbf{a}$ for a (001) superlattice with period $D=LA$, where $L=(u+v)/2$. For simplicity, although this need not be a constraint, we have neglected the small difference in lattice constant between GaAs and AlAs. From Fig. 1(a), the primitive translation vectors of the fcc lattice are

$$\begin{aligned}\mathbf{a}_1'&=(\hat{\mathbf{i}},0,\hat{\mathbf{k}})A/2\ ,\\ \mathbf{a}_2'&=(\hat{\mathbf{i}},\hat{\mathbf{j}},0)A/2\ ,\\ \mathbf{a}_3'&=(0,\hat{\mathbf{j}},\hat{\mathbf{k}})A/2\ ,\end{aligned}\tag{1}$$

and the primitive translation vectors $\mathbf{b}'$ of the reciprocal lattice to the fcc lattice are

$$\begin{aligned}\mathbf{b}_1'&=(\hat{\mathbf{i}},-\hat{\mathbf{j}},\hat{\mathbf{k}})2\pi/A\ ,\\ \mathbf{b}_2'&=(\hat{\mathbf{i}},\hat{\mathbf{j}},-\hat{\mathbf{k}})2\pi/A\ ,\\ \mathbf{b}_3'&=(-\hat{\mathbf{i}},\hat{\mathbf{j}},\hat{\mathbf{k}})2\pi/A\ .\end{aligned}\tag{2}$$

In the case of the superlattice, the primitive translation vectors are

$$\begin{aligned}\mathbf{a}_1&=(\hat{\mathbf{i}},-\hat{\mathbf{j}},0)A/2\ ,\\ \mathbf{a}_2&=(\hat{\mathbf{i}},\hat{\mathbf{j}},0)A/2\ ,\\ \mathbf{a}_3&=(0,0,\hat{\mathbf{k}})LA\ ,\end{aligned}\tag{3}$$

and the primitive translation vectors $\mathbf{b}$ of the reciprocal lattice to the superlattice are

$$\begin{aligned}\mathbf{b}_1&=(\hat{\mathbf{i}},-\hat{\mathbf{j}},0)2\pi/A\ ,\\ \mathbf{b}_2&=(\hat{\mathbf{i}},\hat{\mathbf{j}},0)2\pi/A\ ,\\ \mathbf{b}_3&=(0,0,\hat{\mathbf{k}})2\pi/LA\ .\end{aligned}\tag{4}$$

A general bulk reciprocal lattice vector (RLV) is written

$$\begin{aligned}\mathbf{G}&=h'\mathbf{b}_1'+k'\mathbf{b}_2'+l'\mathbf{b}_3'\\ &=(2\pi/A)(h'+k'-l',-h'+k'+l',h'-k'+l')\end{aligned}\tag{5}$$

and a general superlattice RLV is written

$$\begin{aligned}\mathbf{g}&=h\mathbf{b}_1+k\mathbf{b}_2+l\mathbf{b}_3\\ &=(2\pi/A)(h+k,-h+k,l/L)\ .\end{aligned}\tag{6}$$

We note that $h+k$ and $k-h$ are either both even or both odd. Expressions for $\mathbf{g}$ in terms of the $\mathbf{b}'$ and expressions for $\mathbf{G}$ in terms of the $\mathbf{b}$ can be obtained through simple algebra. The important point to note is that the primitive RLV's for the bulk crystal and for the superlattice cannot be the same. The volume of the unit cell of the superlattice is $\Omega_{SL}=2L\Omega_B$, where $\Omega_B=A^3/4$ is the volume of the unit cell of the fcc lattice.

In Fig. 1(b), we show the first Brillouin zone (BZ) of the $(GaAs)_1(AlAs)_1$ (001) superlattice labeled with the line and points of high symmetry which are of particular interest in this work. The relationship between this BZ and the BZ of the fcc lattice [see Fig. 1(c)] is shown in Fig. 1(d). As the period of the superlattice increases, the height (along k_z) of the superlattice Brillouin zone (SBZ) decreases and the number of times the bulk energy bands have to be "folded" in order to be contained within the SBZ also increases. For example, in the case of the $u=v=1$ superlattice, the bulk bands need only be folded in half. We should add, however, that a superlattice comprises at least two different materials and so the concept of band folding must not be taken too literally. Since the number of atoms and therefore the number of valence electrons contained within the superlattice unit cell is $2L$ times the number of atoms contained within the bulk unit cell, there are $2L$ times as many energy levels in the SBZ as in the bulk Brillouin zone (BBZ).

A. Bulk crystals

We write the one-electron pseudopotential Hamiltonian for the bulk crystal (e.g., GaAs) as

$$H_0=-\tfrac{1}{2}\nabla^2+V_\rho(r)\tag{7}$$

where

$$V_\rho(r)=V(r)+V_R(r)\tag{8}$$

and

$$V_R(r)=\sum_t(E-E_t)\,|\,b_t\rangle\langle b_t\,|\ .\tag{9}$$

$V(r)$ is the true crystal potential and $|\,b_t\rangle$ is a core state with energy E_t. The term V_R involving the core states is an effective repulsive potential and so the matrix elements of V_ρ are correspondingly smaller than those of V. Ignoring the effects of nonlocality, the pseudopotential $V_\rho(r)$

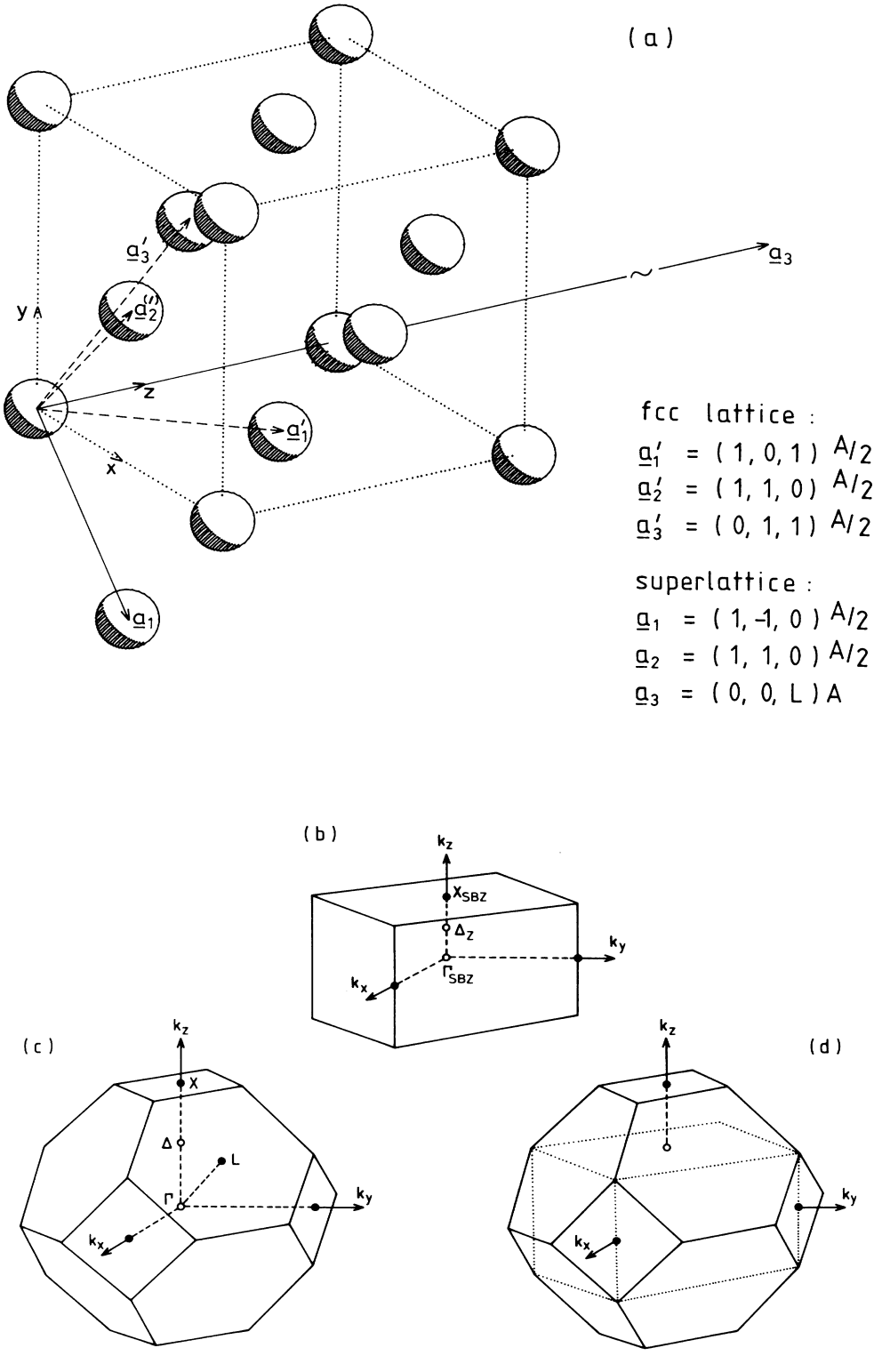

FIG. 1. (a) Diagram showing a set of primitive translation vectors **a**′ for the face-centered cubic (fcc) lattice and a set of primitive translation vectors **a** for an (001) superlattice with period $D = LA$ (see text). (b) Brillouin zone for a $(GaAs)_1(AlAs)_1$ (001) superlattice labeled with the line and points of high symmetry which are of particular interest in this work. (c) Brillouin zone for an fcc lattice. (d) Diagram showing the relationship between the Brillouin zones in (b) and (c).

can be regarded simply as a superposition of local, spherically symmetric atomic pseudopotentials.

For the zinc-blende crystal, the Fourier transform of the pseudopotential may be written as a Fourier sum over RLV's $\mathbf{G}$

$$V_p(\mathbf{r})=\sum_{\mathbf{G}} V_L(\mathbf{G})e^{i\mathbf{G}\cdot\mathbf{r}}\,, \tag{10}$$

$$=\sum_{\mathbf{G}}\sum_{\substack{\text{atomic}\\ \text{species},\alpha}} S_\alpha(\mathbf{G})V_L^\alpha(\mathbf{G})e^{i\mathbf{G}\cdot\mathbf{r}}\,, \tag{11}$$

where $V_L^\alpha(\mathbf{G})$ represents the Fourier transform of the atomic pseudopotential at wave vector $\mathbf{G}$. The structure factor $S(\mathbf{G})$ gives the locations of the atoms within the unit cell;

$$S(G)=\sum_{\mathbf{R}_j} e^{-\mathbf{G}\cdot\mathbf{R}_j}\,, \tag{12}$$

where $\mathbf{R}_j$ is a basis vector to each atom j. The crystal states ϕ are expanded in terms of plane waves and the coefficients of the expansion are determined by requiring that these states satisfy the Schrödinger equation

$$H_0\phi=(-\tfrac{1}{2}\nabla^2+V_p)\phi=E\phi \tag{13}$$

with eigenvalues E.

In fitting the pseudopotential form factors to experimental values of band gaps, we retain only the three lowest independent symmetric and antisymmetric Fourier coefficients which are permitted by symmetry for the zinc-blende crystal. Higher-order Fourier coefficients are neglected on the grounds that the pseudopotential is smooth even into the core regions where the strong repulsive and attractive parts of the true potential nearly cancel (see, for example, Refs. 10 and 11) and so we set $V(|\mathbf{G}|)=0$ for $|G|^2>16$, with $\mathbf{G}$ measured in units of $2\pi/A$.

The effects of spin-orbit coupling are incorporated using an extension[12] of the method introduced by Weisz.[13] The eigenfunctions $\phi_{n\mathbf{k}s}$ and eigenvalues $E_{n\mathbf{k}s}$ of H_0, such that $H_0\phi_{n\mathbf{k}s}=E_{n\mathbf{k}s}\phi_{n\mathbf{k}s}$ are generated by diagonalizing the matrix

$$||\{\tfrac{1}{2}K^2-E_{n\mathbf{k}s}\}\delta_{\mathbf{G},\mathbf{G}'}\delta_{s,s'}+V_L(|\mathbf{G}-\mathbf{G}'|)\delta_{s,s'}+V_{\mathrm{SO}}^{s,s'}(\mathbf{K},\mathbf{K}')||=0\,, \tag{14}$$

where n is the band index, $\mathbf{G}$ is a bulk reciprocal lattice vector, wave vector $\mathbf{K}=\mathbf{k}+\mathbf{G}$, s and s' are spin states, and V_L and V_{SO} are the local and spin-orbit coupling terms.

Since each Bloch function $\phi_{n\mathbf{k}s}(\mathbf{r})$ is defined only to within an arbitrary phase factor, the $\phi_{n\mathbf{k}s}(\mathbf{r})$ are made real and positive at $\mathbf{r}=\mathbf{0}$. The $\phi_{n\mathbf{k}s}(\mathbf{r})$, expanded in terms of plane waves

$$\phi_{n\mathbf{k}s}(\mathbf{r})=\sum_{\mathbf{G}} a_{n\mathbf{k}}(\mathbf{G},s)e^{i(\mathbf{k}+\mathbf{G})\cdot\mathbf{r}}\,|\,s\rangle \tag{15}$$

are normalized so that

$$\langle\phi_{n'\mathbf{k}'s'}\,|\,\phi_{n\mathbf{k}s}\rangle=\delta_{n',n}\delta(\mathbf{k}'-\mathbf{k})\delta_{s',s}\,. \tag{16}$$

The effect of hydrostatic pressure (HP) on the electronic and optical properties of zinc-blende semiconductors is linked directly to the changes induced in the interatomic distances. These changes lead to changes in the charge distributions of the covalent bonds and consequently affect all of the important parameters by which these structures may be characterized. The most important of these parameters are principal energy gaps, effective masses, and oscillator strengths. It is these which play the major role in most descriptions of the optical and transport properties of semiconductors.[14] Changes in the energy gap due to variations in HP are usually determined by measuring the variation in the photon energy at which the absorption edge reaches an arbitrary level. Provided that complications with the shape and intensity of the absorption edge are not encountered, the accuracy of such derivative measurements is likely to be greater than the accuracy of absolute measurements of energy gap.[15] However, no experimental method exists to determine the deformation of the $E(\mathbf{k})$ surface with pressure. Various band structures have been proposed for GaAs and AlAs using the empirical pseudopotential method (EPM).[16–19] However, in order to reproduce band structures which give principal energy gaps for hydrostatic pressures up to at least 50 kbar and which are in as good agreement as possible with experiment, new form factors have been fitted for both GaAs and AlAs. The form factors for GaAs are shown in Table I(a) and the form factors for AlAs are shown in Table I(b). For simplicity, although this need not be a constraint, we have assumed that, at any given pressure, GaAs and AlAs have the same (averaged) lattice constant. The lattice constant A at any pressure P is calculated using the Murnaghan equation of state[20]

$$P=\frac{B_0}{B_0'}\left[\left(\frac{V_0}{V}\right)^{B_0'}-1\right]\,, \tag{17}$$

where B_0 is the bulk modulus at $P=0$ and B_0' is the derivative of B_0 with respect to P. We use a value of 5.654 Å for A_0 and values of 0.754 Mbar and 4.49, respectively, for B_0 and B_0'.[21] For simplicity, we shall refer to atmospheric pressure as 0 kbar. The principal energy gaps of GaAs have been fitted to the recent experimental data of Wolford and Bradley;[22] the calculated and experimental values are compared in Table I(c). The calculated crossing of the Γ_6^c and X_6^c levels occurs at 41.5 kbar. We note that the variation of the band gaps are linear with pressure, consistent with linear deformation-potential theory.[23] This is in contrast with the earlier measurements of Welber *et al.*[24] A recent study has shown that the negative pressure coefficient in GaAs of the X_6^c point with respect to Γ_8^V is attributable to high-

TABLE I. Table giving the pseudopotential local form factors (in atomic units) and lattice constant (in atomic units) for (a) GaAs and (b) AlAs for hydrostatic pressures from atmospheric (0 kbar) to 50 kbar. The only nonzero form factors are the symmetric (S) form factors for $q^2=3$, 8, and 11 and the antisymmetric (A) form factors for $q^2=3$, 4, and 11 (with wave vector q in units of $2\pi/A$). The calculated energies of the principal symmetry points (Γ,X and L) in the lowest conduction band of GaAs and AlAs are given in (c) together with (in parentheses) recent experimental data (Ref. 9 and references therein).

(a)

Pressure (kbar)	Lattice constant (au)	GaAs $S3$	$S8$	$S11$	$A3$	$A4$	$A11$
0	10.683	−0.119 80	0.006 30	0.030 00	0.035 00	0.025 00	0.005 00
10	10.637	−0.119 86	0.007 03	0.030 46	0.035 30	0.025 21	0.004 85
20	10.594	−0.119 88	0.007 75	0.030 93	0.035 60	0.025 42	0.004 70
30	10.553	−0.119 85	0.008 47	0.031 39	0.035 90	0.025 63	0.004 55
40	10.515	−0.119 75	0.009 18	0.031 85	0.036 20	0.025 83	0.004 40
50	10.478	−0.119 65	0.009 88	0.032 32	0.036 51	0.026 04	0.004 25

(b)

Pressure (kbar)	Lattice constant (a.u.)	AlAs $S3$	$S8$	$S11$	$A3$	$A4$	$A11$
0	10.683	−0.115 37	0.012 71	0.035 00	0.036 25	0.031 25	−0.003 75
10	10.637	−0.115 49	0.013 51	0.035 46	0.036 55	0.031 46	−0.003 90
20	10.594	−0.115 52	0.014 31	0.035 93	0.036 85	0.031 67	−0.004 05
30	10.553	−0.115 54	0.015 10	0.036 39	0.037 15	0.031 88	−0.004 20
40	10.515	−0.115 46	0.015 88	0.036 85	0.037 45	0.032 08	−0.004 35
50	10.478	−0.115 38	0.016 65	0.037 32	0.037 76	0.032 29	−0.004 50

(c)

Pressure (kbar)		Γ_6^c (eV)	X_6^c (eV)	L_6^c (eV)
0	GaAs	1.523 (1.522)	2.012 (2.010)	1.846 (1.840)
	AlAs	3.020	2.290	2.661
10	GaAs	1.629 (1.629)	1.997 (1.997)	1.884
	AlAs	3.127	2.277	2.701
20	GaAs	1.737 (1.737)	1.984 (1.984)	1.924
	AlAs	3.235	2.263	2.741
30	GaAs	1.844 (1.844)	1.970 (1.970)	1.962
	AlAs	3.342	2.250	2.782
40	GaAs	1.951 (1.951)	1.956 (1.956)	2.001
	AlAs	3.449	2.236	2.821
50	GaAs	2.058 (2.058)	1.943 (1.943)	2.041
	AlAs	3.556	2.223	2.862

energy d states which depress the X minima.[25]

Unfortunately, only limited data are available on the band structure of AlAs at atmospheric pressure and, to the best of our knowledge, no experiments under HP have been reported for AlAs. We have based the direct and indirect gaps of AlAs at atmospheric pressure on data available in Refs. 26–28 and have assumed that the pressure coefficients of the principal energy gaps are the same as those for GaAs. The calculated energies of the principal symmetry points in the lowest conduction band of AlAs are shown in Table I(c). Where necessary, we use the form factors in Table I and the virtual crystal approximation in order to model the band structure of the alloy $Al_xGa_{1-x}As$.

In Fig. 2(a), we show the lowest conduction band of GaAs (solid curve) and AlAs (dashed curves) between Γ and $X=(0,0,1)2\pi/A$ at atmospheric pressure. The AlAs conduction band has been shown for the cases in which 85% and 60% of the difference between the band gaps in Table I at Γ of GaAs and AlAs is taken up as the discontinuity between the two Γ_6^c levels. These two band offsets will be considered as limiting cases throughout this paper. We shall refer to the lowest conduction band as CB1; other bands to which reference will be made are (i) the split-off band; VB2, (ii) the light-hold band; VB3, (iii) the heavy-hole band; VB4, and (iv) the second conduction band; CB2. Since spin-orbit coupling has been included, each of the bulk bands is doubly degenerate.

In Fig. 2(b), we show how the lowest conduction band in the band structure of GaAs is deformed as HP is increased from 0 to 50 kbar. It can be seen that as HP is increased, the principal minimum at Γ moves up in energy and the secondary minimum near X moves down in energy. It should be noted that the secondary minimum does

not lie exactly at the edge of the BZ (see Fig. 2). Apart from studies such as those by Carter *et al.*,[29] there appears to be no experimental information in the literature on the position, depth, or width of the camel's back in either GaAs or AlAs. The significance of this feature in the bulk band structures will be discussed later within the context of superlattice band structures.

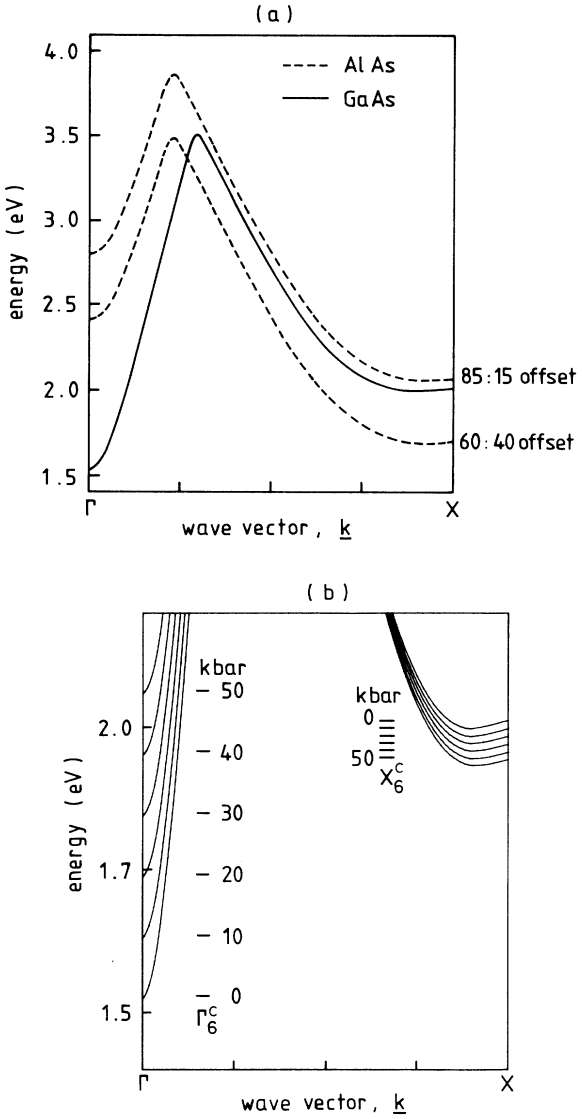

FIG. 2. (a) The lowest conduction band of GaAs (solid curve) and AlAs (dashed curves) along the Δ line between Γ and $X=(0,0,1)2\pi/A$ at atmospheric pressure. The AlAs conduction band has been shown for the cases in which 85% and 60% of the difference between the band gaps at Γ in Table I of GaAs and AlAs is taken up as the discontinuity between the two Γ_6^c levels. (b) Variation with hydrostatic pressure of the lowest conduction band of GaAs between Γ and $X=(0,0,1)2\pi/A$. Hydrostatic pressure of 0 kbar is used to denote atmospheric pressure. The crossing of the Γ_6^c and X_6^c levels occurs at 41.5 kbar, in accordance with the experimental data of Wolford and Bradley (Ref. 22).

The effective mass m^* of the ground electron state at Γ_6^c as a function of HP has been calculated using the expansion[30]

$$\frac{1}{m^*}=1+2\sum_{\substack{n\\ n\neq n'}}\frac{|\mathbf{e}\cdot M_{n'n}|^2}{E_{n'}-E_n}\ , \tag{18}$$

where $\mathbf{e}$ is a unit vector lying in the [001] direction, $M_{n'n}=\langle\phi_n|\hat{\mathbf{P}}|\phi_{n'}\rangle$ is the momentum matrix element with $\hat{\mathbf{P}}=-i\nabla$ the momentum operator and ϕ_n the bulk Bloch function belonging to band n. In Table II, we show our calculated values of m^* and pressure coefficient $M_P=(1/m^*)(dm^*/dP)$; where possible, comparison has been made with other values in the literature.[17,18,31–37]

B. Superlattices

The superlattice is viewed as a host crystal in which monolayers are periodically substituted with a different material. We expand the superlattice wave function Ψ on a complete set of host-crystal eigenfunctions in the reduced-zone representation

$$\Psi=\frac{1}{\sqrt{\Omega}}\sum_{n,\mathbf{k},s}A_{n\mathbf{k}s}\phi_{n\mathbf{k}s} \tag{19}$$

and write the superlattice Schrödinger equation

$$(H_0+V)\Psi=E\Psi\ . \tag{20}$$

The dependence of Ψ on $\mathbf{k}$ within the SBZ is implicit. The term V represents the difference in potential at all relevant sites between the atoms of the host crystal and

TABLE II. Table showing calculated and experimental values for the effective mass m^* and the pressure coefficient $M_P=(1/m^*)(dm^*/dP)$ for the electron state at Γ_b^c. The units of m^* are m_e and the units of M_P are Mbar^{-1}.

		This work	Other calculated values	Experimental values
GaAs	m^*	0.0772	0.075[a] 0.067[b] 0.078[c]	0.0648[d] 0.067[e]
	M_P	5.44	6.8±0.3[f]	7.0[g] 6.5[g]
AlAs	m^*	0.143	0.110[a] 0.22[b] 0.15[h] 0.15[i]	
	M_P	2.11		

[a]Braunstein and Kane, Ref. 31.
[b]Lawaetz, Ref. 32.
[c]Neumann *et al.*, Ref. 17.
[d]Chamberlain and Stradling, Ref. 33.
[e]Vrehen, Ref. 34.
[f]Christensen, Ref. 35.
[g]Pitt *et al.*, Ref. 36.
[h]Stukel and Euwema, Ref. 37.
[i]Hess *et al.*, Ref. 18.

the atoms which are substituted in their place. The set of $\mathbf{k}$ points included in the expansion of Ψ is determined by the periodicity of the superlattice and is therefore unique. Multiplying Eq. (20) from the left by $(1/\sqrt{\Omega})\phi^*_{n'\mathbf{k}'s'}$ and integrating over the volume of the crystal, we are left with a set of linear equations

$$A_{n'\mathbf{k}'s'}(E_{n'\mathbf{k}'s'}-E)+\frac{1}{\Omega}\sum_{n,\mathbf{k},s}A_{n\mathbf{k}s}\langle\phi_{n'\mathbf{k}'s'}\mid V\mid\phi_{n\mathbf{k}s}\rangle=0\ , \tag{21}$$

the solutions of which are obtained by direct diagonalization. For the remainder of this paper, we shall, for simplicity, drop the subscript s used to denote the spin variable.

It should be noted that we are solving an integral equation and so avoid the necessity of imposing boundary conditions for the matching of wave functions (see, for example, Refs. 38–41).

Since a complete atomistic description of the superlattice is used, the full space group of the superlattice is automatically included and so results consistent with group theory are obtained.

III. SUPERLATTICES: RESULTS AND DISCUSSION

A. Numerical aspects of the calculations

In this section we consider the convergence properties of our pseudopotential method and the numerical uncertainties involved in the calculation of (superlattice) electronic states. Since the electronic states are expanded in terms of functions which are closely related to the "Bloch waves" of the superlattice system, the secular matrices which have to be solved have smaller dimensions compared with a direct band-structure calculation using a plane-wave basis set. Besides having the proper behavior at the host-atom sites, the basis functions closely resemble the true solutions at the substitute-atom sites. Since the method of calculation is one in which energy levels are calculated with respect to some reference levels, i.e., the energy levels of the host crystal, the errors are much smaller than those, about 100 meV, normally encountered in supercell (large-unit cell) calculations in which all energies are calculated on an absolute scale.

In the present calculations, the worst possible errors are those associated with the calculation of the band structure of one material, e.g., AlAs, having expanded the (superlattice) states Ψ in terms of the Bloch functions of another material, e.g., GaAs. Since AlAs is an indirect gap material and GaAs is a direct gap material, the calculation of the band structure of, say, AlAs from the band structure of GaAs represents an especially difficult test of numerical accuracy. Another feature of this calculation is that the potential associated with every atom in the unit cell is changed, which is in contrast with the usual superlattice calculation in which the potential associated with only some of the atoms may be affected. It is this particular calculation which we shall consider in detail.

We expand Ψ in terms of five bands, (VB2, VB3, VB4, CB1, and CB2) of GaAs at Γ,X. The fact that each band is two-fold spin degenerate is implicit. The offsets used in the calculation are the so-called 60:40 offsets in which 60% of the difference in band gaps at Γ_6^c between GaAs and AlAs is taken up as the offset in the conduction band.

In Table III(a), we show the energies at Γ,X of GaAs and the calculated and expected energies at Γ,X of AlAs for the case of 60:40 offsets. The numbers obtained by expanding Ψ on the eight lowest bands in the band structure of GaAs are very similar to those shown in Table III(a). We note that at least 65 waves must be used in the expansion of each host-crystal state. It was found that no numerical advantage was obtained by using double rather than single-precision arithmetic. From Table III(a), it can be seen that the maximum error associated with the calculation of an AlAs level at Γ or X is about 50 meV and that this pertains only to the levels in the conduction band. In the case of 60:40 offsets, the error in the calculated energy of the X_6^c (AlAs) level is 47 meV but this reduces almost linearly with decreasing alloy concentration x. The error in the calculation of the valence-band levels of AlAs is very small, a reflection of the usual rig-

TABLE III. (a) Table showing energies in eV at Γ,X of GaAs and the calculated and expected energies at Γ,X of AlAs for the case of 60:40 offsets. The energy levels of AlAs have been calculated by exchanging every GaAs monolayer in the host crystal with an AlAs monolayer. (b) Table showing energies in eV which are analogous to those in (a) for the case in which AlAs is used as the host crystal.

(a)

Level	GaAs (input)	AlAs (output) expected	AlAs (output) obtained	difference
Γ_6^c	1.523	2.421	2.473	0.052
Γ_8^v	0.108	−0.502	−0.490	0.012
Γ_7^v	−0.226	−0.798	−0.790	0.008
X_6^c	2.012	1.691	1.738	0.047

(b)

Level	AlAs (input)	GaAs (output) expected	GaAs (output) obtained	difference
Γ_6^c	2.421	1.523	1.582	0.059
X_6^c	1.691	2.012	2.053	0.041

idity of valence bands calculated within the empirical pseudopotential scheme (see, for example, Ref. 16).

On the basis of the results shown in Table III(a), we suggest that any significant errors involved in the calculation of states in GaAs-$Al_xGa_{1-x}As$ (001) superlattices are associated only with the states in the conduction band. The error associated with states in the valence band is likely to be no more than 1—3 meV. In the remainder of this discussion on convergence properties and numerical uncertainties, we shall therefore be concerned only with conduction-band states; this will be assumed implicitly.

Depending on the sensitivity of particular superlattice states to the band offset, the errors associated with such states may be much smaller than about 50 meV. For example, the error in the energy of the ground conduction Γ-related bound state in a GaAs-$Al_xGa_{1-x}As$ (001) superlattice with $x \lesssim 0.4$ may be less than about 2 meV since the Γ_6^c barrier is itself no more than about 400 meV in height. Also, since the camel's back structure near X traps at least one pair of bound states for layers of width greater than about 30 Å (e.g., Ref. 8), the error associated with the position of such states within the camel's back can be no more than about 4 meV. In such cases where two or more levels are almost degenerate, the computer may return linear combinations of the true wave functions. Physically meaningful quantities such as charge densities and optical matrix elements are necessarily sums over the relevant degenerate states.

It should be noted that if AlAs Bloch states are used in the expansion of Ψ, the typical errors shown in Table III(a) will correspond to the energies of GaAs levels. In order to illustrate this, we show in Table III(b) the results of a calculation using 60:40 offsets in which the energies of the Γ_6^c and X_6^c levels in CB1 of GaAs are calculated using expansions in terms of Γ and X states of AlAs. It is important to realize that, although the energy of a given superlattice state may have an error of between 1 and 50 meV, both the *magnitude* and the *sign* of this error can nearly always be determined using information such as that given in Table III. The uncertainty in any given energy level is therefore much smaller than would on first inspection be expected from the data given in Table III. In order to obtain the best results for a given superlattice, it is helpful to choose a basis set which gives rise to the least numerical uncertainty for those superlattice states which are of particular interest.

In order to change the relative alignment of the two bulk band structures (to give either an 85:15 or a 60:40 offset), different analytic fits to the empirical pseudopotential form factors have been used. In reality, the actual offset is influenced by transfer of charge between the two materials which takes place in a narrow region at the interface. Such an effect, notoriously difficult to establish quantitatively,[42] has its origins in both small and large wave vector (q) components of the potential. We temporarily circumvent this problem by adjusting only the small q components of the potential, an approximation which will be examined in detail in subsection C.

We have carried out a series of tests which show that, for superlattices in which the layer widths are greater than about 30 Å, any uncertainty in the potential at wave vectors lying far from the bulk RLV's is immaterial and that smooth truncation of the potential at about $q^2 = 64\pi^2/A^2$ leads to results which are effectively stable;[43,44] the case of ultrathin layers is more complicated and has been described elsewhere.[8] In addition to the component of the superlattice potential at the bulk RLV with $q=0$, it is the Fourier components at and clustered around the bulk RLV's which play the leading role in determining the charge densities. It is for these reasons that self-consistency does not appear to be a stringent requirement for the calculation of the electronic and optical properties of superlattice structures whose layers comprise a few or more lattice constants. Charge redistribution between the layers is restricted to a narrow region at the interfaces and the resultant sheet of redistributed charge controls an effectively sharp step in potential. Our pseudopotential method can therefore be used to fit transition energies from experimental data to within a few meV despite the uncertainties in the long-wavelength Fourier components of the superlattice potential.[5]

B. Basic electronic structure

It is instructive to see how the confined states are directly related to the bulk Bloch states on which they are expanded and how their properties depend on the constituent materials of the superlattice. We consider a superlattice with 60:40 offsets of period $D = 27A$ comprising (GaAs,51 Å/$Al_xGa_{1-x}As$,102 Å; $0 \le x \le 1.0$). Specifically, the GaAs layer comprises 18 monolayers and the alloy layer comprises 36 monolayers. We expand Ψ at Γ_{SBZ} in terms of GaAs Bloch states. The states which are included in Ψ are those belonging to $\mathbf{k}$ points in the BBZ which are coupled to Γ_{SBZ} by some linear combination of $\mathbf{g}$'s. In this case, the only $\mathbf{g}$'s which are coupled to Γ_{SBZ} are those of the form $(0,0,\pm 0.037p)2\pi/A$, where p is a positive integer. For simplicity, we focus only on the lowest conduction band CB1 in GaAs and so only those superlattice conduction states lying close to the edge of the conduction band of GaAs. We stress, however, that our pseudopotential method is formally a full-zone, multiband method and not a single-band method, although on occasions (as here) it may be adequate to use a single-band approximation.

In Fig. 3(a), we indicate the $\mathbf{k}$ points nearest to Γ which are included in the expansion of Ψ and in Fig. 3(b), we show the charge densities of the corresponding GaAs Bloch states. The charge densities have a modulation length which is equal to $2\pi/k$. Apart from the single state shown for the Γ point, all of the other Bloch states occur in pairs and correspond to linear combinations of the degenerate states at $\mathbf{k}$ and $-\mathbf{k}$. Figure 3(a) also shows the relationship between the lines of the BBZ and SBZ for this superlattice and indicates how the band structure of GaAs in the BBZ may be viewed as a folded band structure in the SBZ. In Figs. 4(a)—4(d), we show how the superlattice states evolve as the proportion of Al in the $Al_xGa_{1-x}As$ region is increased. Figure 4(a) corresponds to the case with $x=0.01$, Fig. 4(b) corresponds to the case with $x=0.1$, Fig. 4(c) corresponds to the case with $x=0.35$, and Fig. 4(d) corresponds to the case with $x=1.0$. The energy levels of these states for x ranging

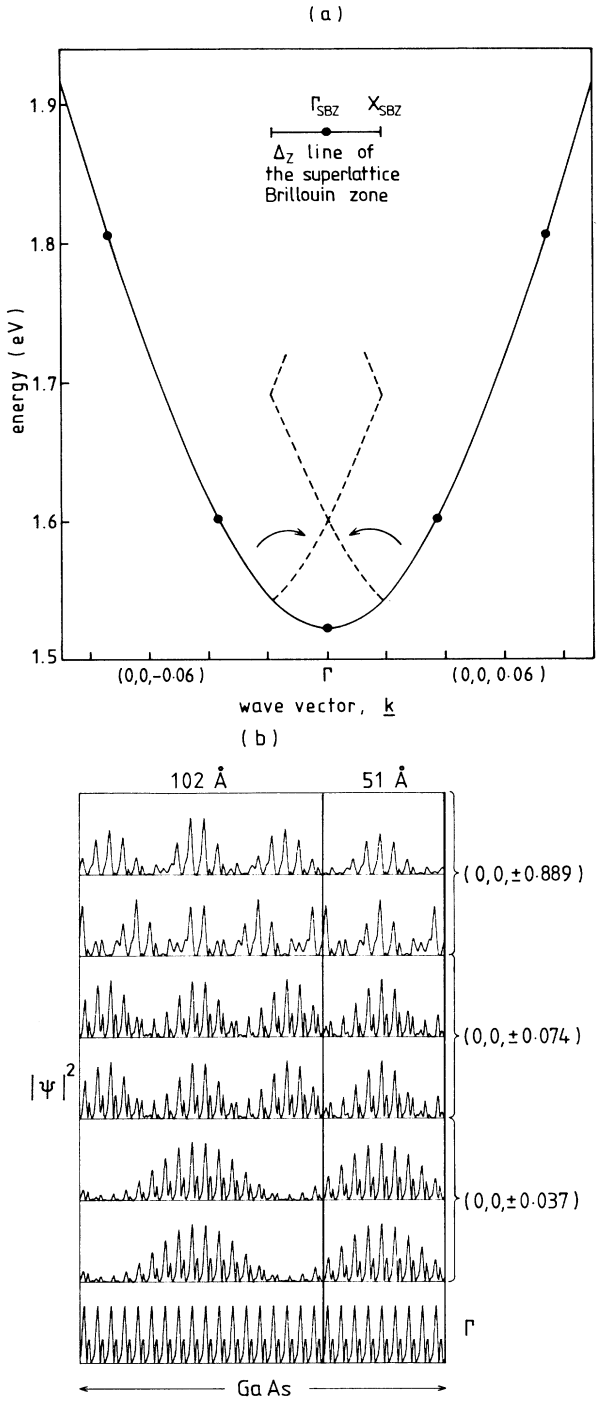

FIG. 3. (a) Section of the lowest conduction band of GaAs at 0 kbar in the vicinity of Γ. Sampling points for a period comprising 27 lattice constants are shown together with the relationship between the Δ_z line of the superlattice Brillouin zone and the folded bands of GaAs. (b) Charge densities of bulk GaAs conduction states of lowest energy at sampling points along the Δ line between Γ and $X=(0,0,1)2\pi/A$ for a superlattice comprising 27 lattice constants. The peak of each charge density $|\Psi|^2$, plotted in the [001] direction, is set to one to facilitate presentation. The origin is in the center of the 51-Å layer. The wave vectors in units of $2\pi/A$ are indicated on the right-hand side of the figure.

from 0 to 1.0 are shown in Fig. 5 and in Fig. 6, we show the sum over spin of the modulus squared of the A_{nks} coefficients in the expansions of the states for the case with $x=0.1$. It should be noted that the superlattice actually comprises two materials but the expansion Ψ is in terms of Bloch states from only one of the materials. Although Ψ in this case has been expanded on GaAs Bloch states, the results which are shown are similar to those which would be obtained if $Al_xGa_{1-x}As$ Bloch states had been used as the basis set. By comparing Fig. 4 with Fig. 5, it can be seen that the conduction states (prefixed with E) group into two types. Firstly, there are those states (labeled symbolically with Γ) which are derived primarily from the center of the BBZ and secondly, there are those states (labeled symbolically with X) which are derived primarily from the edges of the BBZ. For brevity, we shall distinguish between the two types of states using the terms Γ related and X related although one should bear in mind that these states are not derived precisely from just the Γ point or just the X points in the BBZ. It can be seen from Fig. 5 that certain Γ-related states lie above the Γ_6^c ($Al_xGa_{1-x}As$) level. In the sense of the Kronig-Penny model, these states are anti-well states. We shall refer to them as resonances and introduce an additional label R. Thus, for example, the label EXR4 would correspond to the third-excited resonant conduction state derived from bulk components lying at or close to the edges of the BBZ.

It can be seen from Fig. 6 that, apart from the lowest state EΓ1, the states group into pairs with the peaks in the spectral distributions moving progressively away from Γ with increasing energy. The double peak in the spectral distribution of state EΓR1 reduces to a single peak centered on Γ as alloy composition increases causing state EΓR1 to move away from state EΓ2. It should be noted that the peaks in the spectral distribution of state EX1 are centered on the minimum near X. The reason for the apparent double degeneracy of state EX1 will be discussed later.

In Fig. 7(a), we show plots of the leading A_{nks} coefficients, i.e., those from CB1, in the spectral distributions of the lowest conduction states in the (GaAs,51 Å/AlAs,102 Å) superlattice. State EΓ1 and the lowest X-related states are fairly distinct although strong mixing between EΓ2 and EX10 is evident. In Fig. 7(b), we show the charge densities of the strongly mixed EΓ2 and EX10 states. These charge densities (as all other charge densities presented in this paper) have been plotted along a line in the [001] direction passing through mid-bond positions. Although the Γ-X mixing is very strong, it is fairly easy to distinguish between the rapidly varying components of the charge densities which are characteristic either of a Γ-related or an X-related state. This distinction is of course apparent because the bound X-related state is confined almost entirely in the AlAs layer and the bound Γ-related state is confined mostly in the GaAs layer. Γ-X mixing similar to that shown in Fig. 7 can occur between resonant Γ-related and bound X-related states.[4]

By comparing Figs. 3, 4, 5, 6, and 7, it can be seen how the superlattice states evolve from the bulk GaAs states. As the alloy composition x increases from 0, the lowest

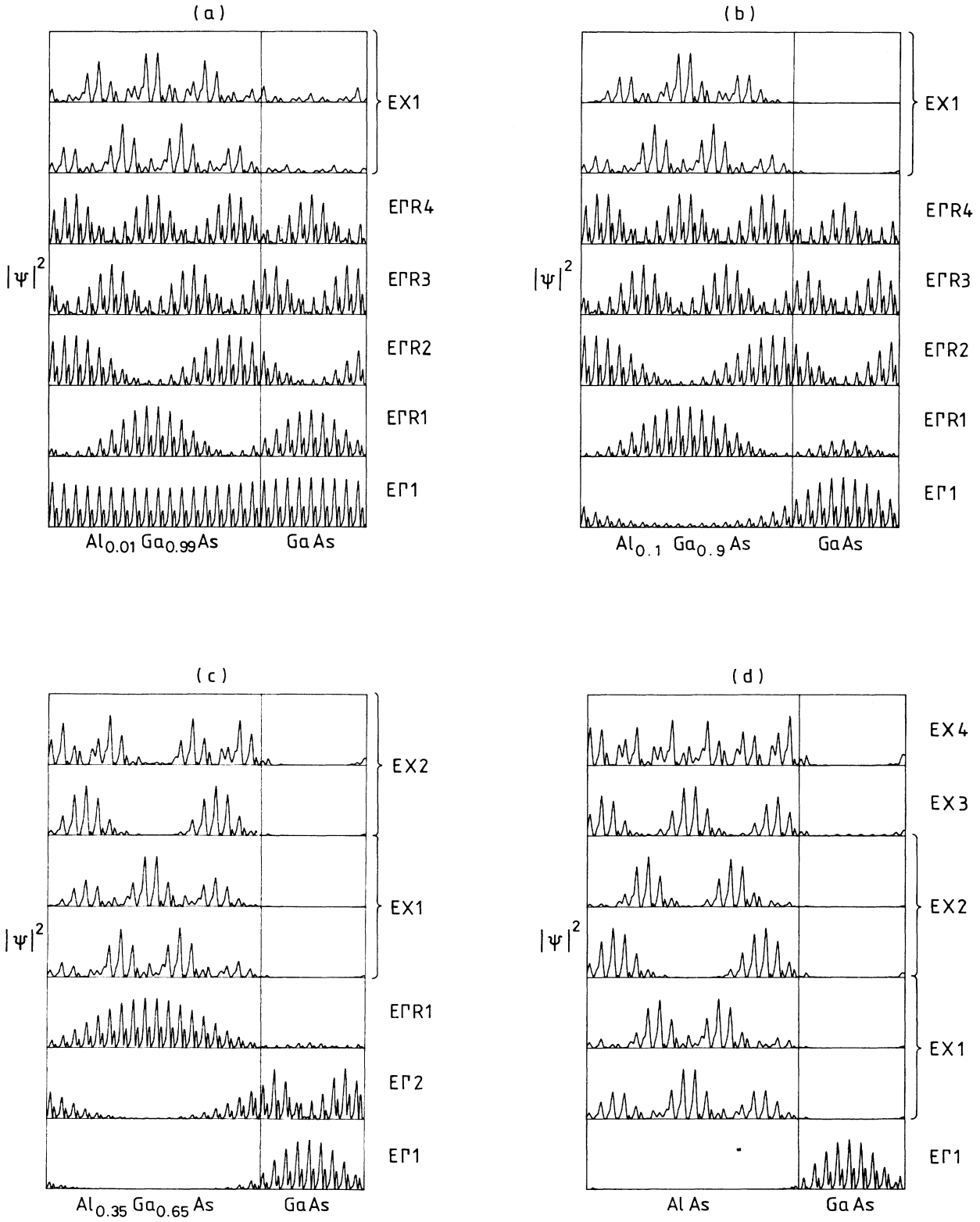

FIG. 4. Electron charge densities plotted along the superlattice axis in the [001] direction, at the center of the superlattice Brillouin zone, in the (GaAs,51 Å/$Al_xGa_{1-x}As$,102 Å) superlattice with 60:40 offsets at 0 kbar. The aluminum fractions x are (a) 0.01, (b) 0.1, (c) 0.35, and (d) 1.0. See the text (Sec. III B) for a classification of the states.

Γ-related state EΓ1 slowly becomes confined in the GaAs layer although there is always remnant tunneling in the alloy layer. The variation in energy with x of state EΓ1 has been shown in Fig. 5 for two cases: one (full curve) in which 60% of the difference between the band gaps of GaAs and $Al_xGa_{1-x}As$ at Γ_6^c is taken up as the conduction-band offset and the other (dashed curve) in which 85% of this difference is taken up as the conduction-band offset. Both the general form of the EΓ1 energy curves and the difference between the 60% and 85% curves can be understood in terms of a simple particle-in-a-box model.

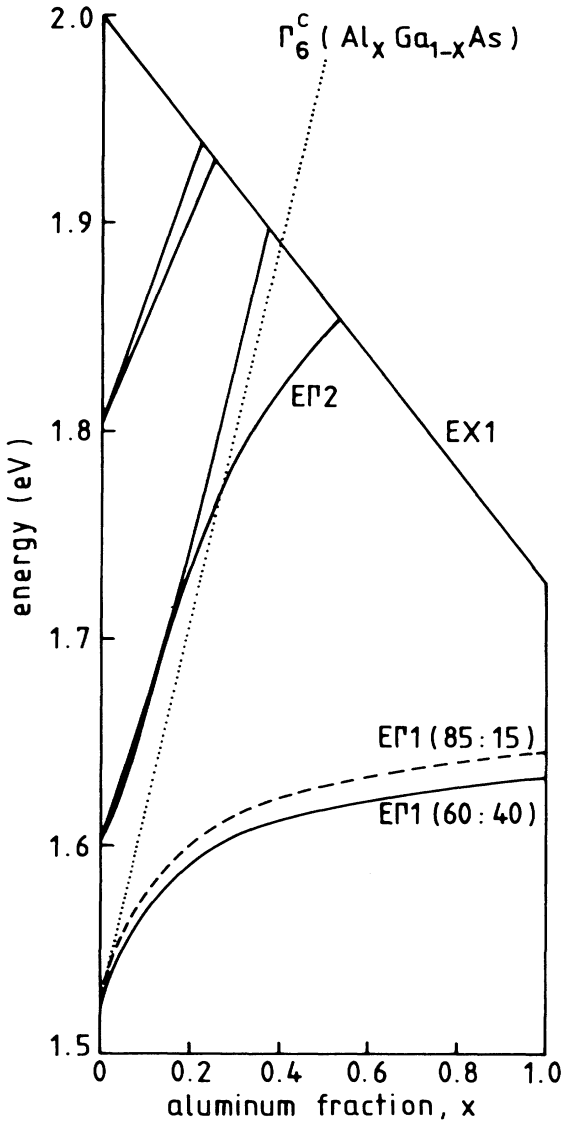

FIG. 5. Variation with aluminum fraction x of the energies of the lowest conduction states, at the center of the superlattice Brillouin zone, in the (GaAs,51 Å/$Al_xGa_{1-x}As$,102 Å) superlattice with 60:40 offsets at 0 kbar. Apart from state EX1, the ground zone-edge-related state confined in the $Al_xGa_{1-x}As$ layers, all of the states shown are zone-center-related states. At any given aluminum fraction, those zone-center-related states lying above the $\Gamma_6^c(Al_xGa_{1-x}As)$ level (shown dotted) are resonant states. At $x=0$, corresponding to bulk GaAs, the states correspond to those shown in Fig. 3. The dashed curve shows the variation in energy of the ground zone-center-related state EΓ1 with 85:15 offsets.

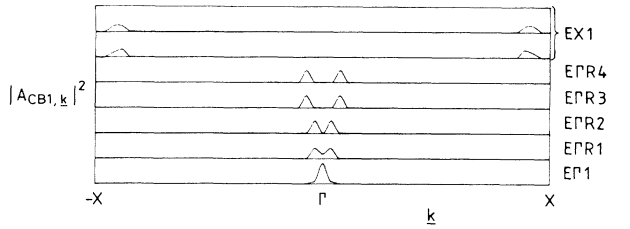

FIG. 6. Plot of $|A_{nks}|^2$ associated with the six lowest conduction states from Fig. 4(b) and from Fig. 5 at $x=0.1$ as a function of k_z along the Δ line of the GaAs Brillouin zone. Only contributions from the lowest bulk conduction band [see Fig. 2(a)] are shown.

For $x \gtrsim 0.25$, the first excited bound (GaAs)-related state EΓ2 is easily distinguishable from the ground resonant ($Al_xGa_{1-x}As$)-related state EΓR1. However, for $x \lesssim 0.25$, the anticrossing states originating primarily from $k=(0,0,\pm 0.037)2\pi/A$ are rather delocalized. Confinement of these states becomes more apparent once state

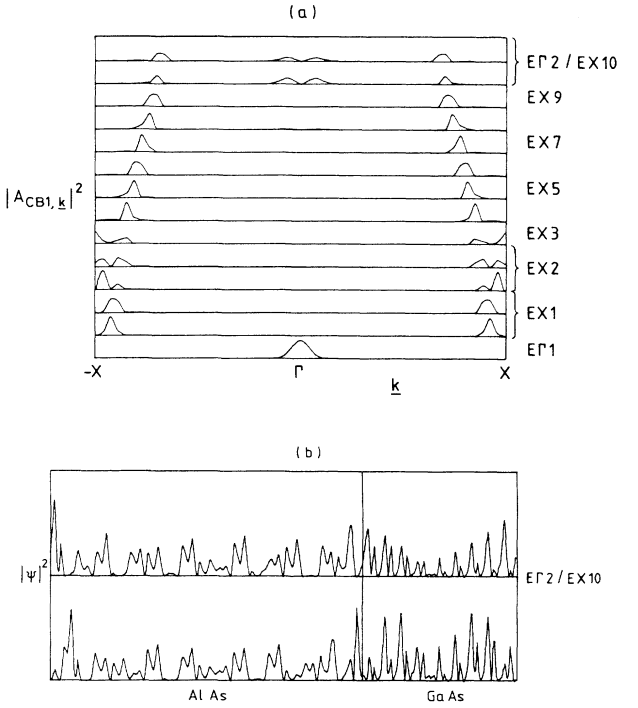

FIG. 7. (a) Plot of $|A_{nks}|^2$ associated with the twelve lowest conduction states from Fig. 4(d) and from Fig. 5 at $x=1.0$ as a function of k_z along the Δ line of the GaAs Brillouin zone. Only contributions from the lowest bulk conduction band are shown. States EΓ2 and EX10 show strong mixing. (b) Charge densities plotted along the superlattice axis in the [001] direction of the two strongly mixed states EΓ2 and EX10 from (a).

$E\Gamma 2$ has been "captured" by the Γ_6^c well and state $E\Gamma R1$ begins to be pushed up by the rising $\Gamma_6^c(Al_xGa_{1-x}As)$ level. The midpoint of the anticrossing occurs at $x=0.16$. In contrast with the gradual process of confinement of the Γ-related states, confinement of the X-related states is abrupt. It can be seen from Fig. 4(b) that complete confinement of the lowest pair of quasidegenerate X-related states has occurred with an alloy concentrate of only 10%.

We show in Fig. 8 the dispersion in the k_z direction of the lowest conduction states in the (GaAs,51Å/$Al_xGa_{1-x}As$,102Å) (001) superlattice for the case of (a) $x=0.01$ and (b) $x=0.35$. The resemblance between the dispersion curves in Fig. 8(a) and the folded bands of GaAs in Fig. 3(a) is apparent. Figure 8(b) shows that there is practically no dispersion on the $E\Gamma 1$ state with $x=0.35$. This lack of dispersion is due to the thick alloy barrier. It can also be seen that the lowest X-related states, strongly confined in the alloy layers [see Fig. 4(c)], also have negligible dispersion and show an increasing spacing with increasing energy. Qualitatively similar behavior would be found using a simple square-well model.

Since the zone-edge-related states have little dispersion in the k_z direction, their velocity along the superlattice axis must be negligible, although some leakage of the states into the barrier regions occurs due to Γ-X mixing. Interaction between the Γ-related and X-related states can significantly modify the dispersions (effective masses) of the states. For example, Fig. 8(b) shows that such an interaction has led to a negative bowing of $E\Gamma R1$ near X_{SBZ}. Such effects, occurring in the hot-electron range of energies, are likely to be important for device physics.

In order to illustrate the effects of varying band offsets on the electronic states other than the ground Γ-related bound state, we show in Fig. 9 the energies of the lowest conduction states at the center of the SBZ in the (GaAs,51Å/$Al_{0.2}Ga_{0.8}As$,102 Å) superlattice for (a) 60:40 offsets and (b) 85:15 offsets. In the spirit of the Kronig-Penny model, "potential wells" have been drawn using the Γ_6^c and lowest Δ_5-minimum bulk levels to highlight the different relative positions of the bulk band structures. However, it is important to realize that for a given offset the difference in energy between two, say, Γ_6^c levels does not represent a step in potential energy. The potential wells drawn in Fig. 9 are effective potential wells (EPW's). The only physical step in potential energy in going from one material to the other is that associated with the difference between the average electrostatic potential energies of the two materials.

By comparing Fig. 9(a) with Fig. 9(b), it can be seen that, in our calculations, the sign of the Δ_5-EPW changes so that in the case of 60:40 offsets the alloy layer is the active region[45] and in the case of 85:15 offsets the alloy layer is the barrier region. This situation was created deliberately by fitting the band structure of AlAs to aver-

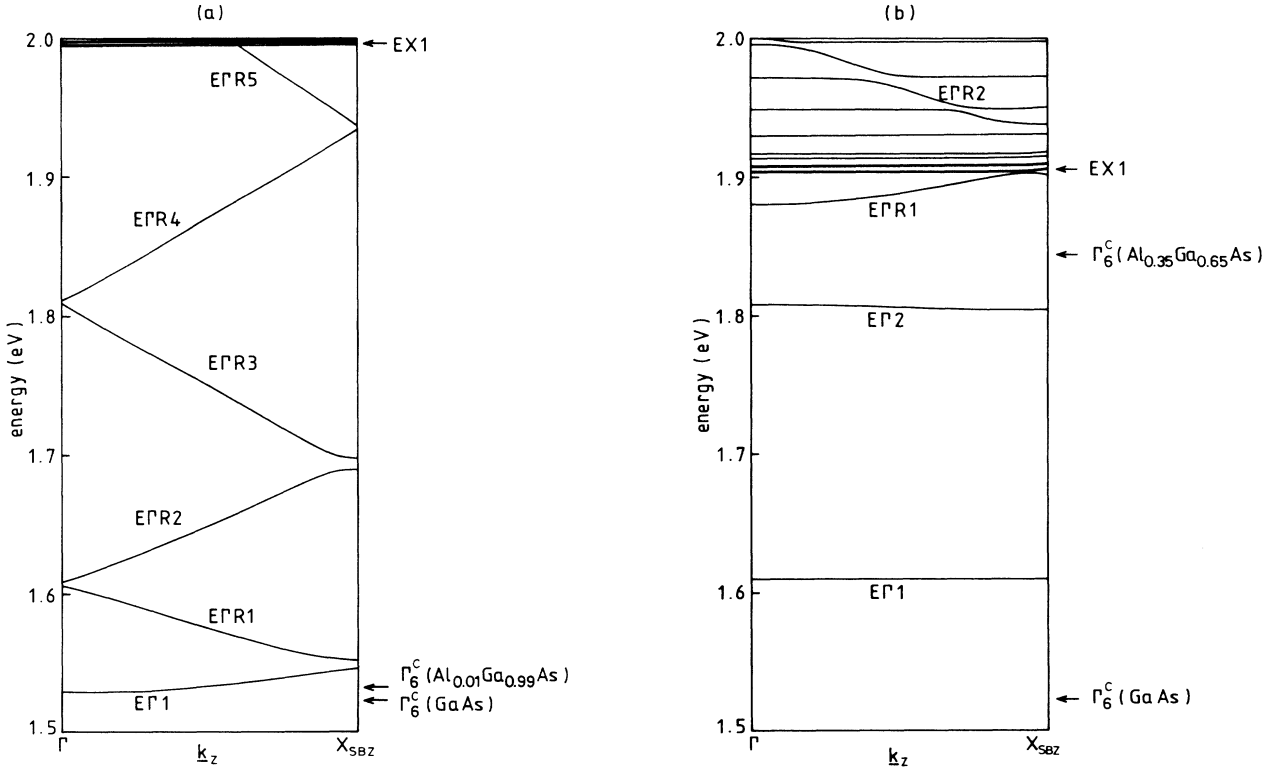

FIG. 8. Dispersions along the Δ_z line between Γ and X_{SBZ} [see Fig. 3(a)] in the superlattice Brillouin zone of the lowest conduction states in the (GaAs,51 Å/$Al_xGa_{1-x}As$, 102 Å) superlattice with 60:40 offsets at 0 kbar with (a) $x=0.01$ and (b) $x=0.35$. In both cases, the lowest zone-edge-related states $EX1$ and $EX2$ (not labeled) each correspond to a pair of quasidegenerate states confined in the alloy layer (see Fig. 4).

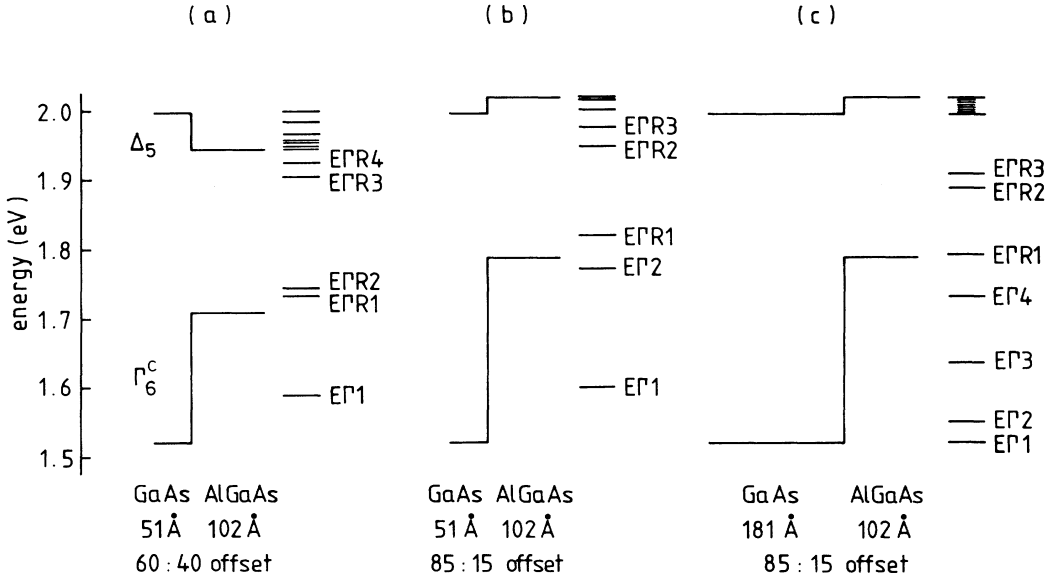

FIG. 9. Energies of the lowest conduction states at the center of the superlattice Brillouin zone in (a) the (GaAs,51 Å/$Al_{0.2}Ga_{0.8}As$,102 Å) superlattice with 60:40 offsets, (b) the (GaAs,51 Å/$Al_{0.2}Ga_{0.8}As$,102 Å) superlattice with 85:15 offsets, and (c) the (GaAs,181 Å/$Al_{0.2}Ga_{0.8}As$,102 Å) superlattice with 85:15 offsets. The effective potential wells associated with the Γ_6^c levels and the lowest point of the Δ_s minima in GaAs and $Al_{0.2}Ga_{0.8}As$ are indicated on the left of each set of energies.

aged values of experimentally determined energy gaps which were adjusted slightly and was done to avoid any ambiguity over the sign of the Δ_5-EPW. Bearing in mind the spread in the experimental data of AlAs, such an approximation does not seem significant. In the case of an exact alignment of the X_6^c levels, we find that complicated interference effects arising from the different Δ_5 minima give rise to charge densities which are peaked at the interfaces.

From Figs. 9(a) and 9(b), it can be seen that in going from 85:15 to 60:40 offsets, the energies of all of the states drop. The Γ-related states, both bound and resonant, drop because the Γ_6^c-EPW becomes shallower and the X-related states drop because the sign of the Δ_5-EPW reverses. Although the Γ-related states remain localized (but less confined) in the same material, the lowest X-related states switch to being localized in the alloy layer rather than in the GaAs layer. The competing effects of active and barrier layers on the energies of Γ-related bound states in GaAs-$Al_xGa_{1-x}As$ (001) superlattices have been studied in detail by Ivanov and Pollmann using a resolvant method based on Green's functions.[46] As the height of the Γ_6^c-EPW decreases, a Γ-related bound state can tunnel further into the (finite) barrier region thus leading to a reduction in its kinetic energy. This tunneling leads to an interaction between the active and barrier regions and a lowering of the energy of the superlattice state. Since Ivanov and Pollman considered only bound states, we show in Fig. 9(c) the energy levels of the lowest conduction states at the center of the SBZ in the (GaAs,181 Å/$Al_{0.2}Ga_{0.8}As$,102 Å) (001) superlattice with 85:15 offsets. The charge densities of the Γ-related states shown in Fig. 9(c) are given in Fig. 10. By comparing

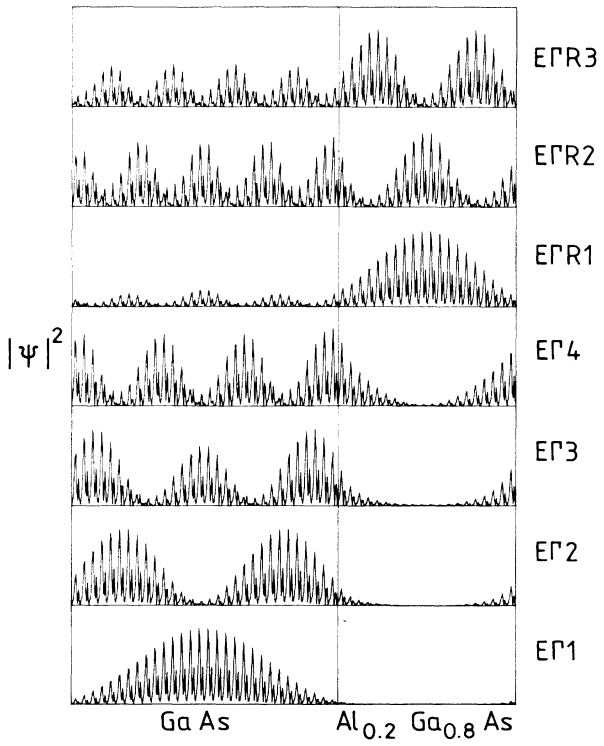

FIG. 10. Charge densities of the lowest conduction states from Fig. 9(c) plotted along the superlattice axis in the [001] direction.

Fig. 9(b) with Fig. 9(c), it can be seen that the number of bound states has increased with the increase in the width of the GaAs layer. The width of the alloy (barrier) layer is the same in both cases. Although Ivanov and Pollmann demonstrate that the GaAs layer predominately determines the number of bound superlattice subbands, it is clear from Figs. 9(b) and 9(c), that it can also influence the position of the resonant states.

It is apparent that the band structure of the superlattice in the range of energies near the X points of the bulk crystals is unlike that associated with the Γ_5 minima. The quasidegeneracies arise as a result of the camel's backs near X and $-X$ in the bulk band structures. To demonstrate this, we have performed calculations in which information about the camel's backs is removed by adjusting manually the energy levels E_{nks} [see Eq. (21)] at and near $\pm X$ in the band structure of the host crystal. We find that removal of the camel's back near $\pm X$ results in the breaking of the quasi-twofold degeneracies. We conclude that the quasidegenerate X-related states found in the $\langle 001 \rangle$ superlattices arise from the equivalent minima lying in from $\pm X$ on the Δ line.

C. Effects of hydrostatic pressure

In our study of the effects of HP on the electronic and optical properties of GaAs-$Al_xGa_{1-x}As$ (001) superlattices, we shall consider two different systems with GaAs layers of width 51 Å. The widths of the alloy layers in these superlattices are 6 and 102 Å at 0 kbar. These superlattices have been chosen in order to highlight several important features. Firstly, results for the (GaAs,51 Å/$Al_xGa_{1-x}As$,102 Å) superlattice with $x=0.25$ and $x=1.0$, together with results presented earlier, are used to illustrate the general effects of HP and make a direct comparison between the effects of alloying and HP. Secondly, results for the (GaAs,51 Å/AlAs,6 Å) superlattice are used to illustrate the response to HP of electronic states which are formed within a layer which is only quasi-bulk-like.

In Fig. 11, we show the variation with HP of the energy of the lowest conduction states at the center of the SBZ in the (GaAs,51 Å/$Al_xGa_{1-x}As$,102 Å) superlattice with (a) $x=0.25$ and (b) $x=1.0$. The calculations have been performed using GaAs Bloch states in the expansion of Ψ for the case of 60:40 offsets. In Table IV, we give the pres-

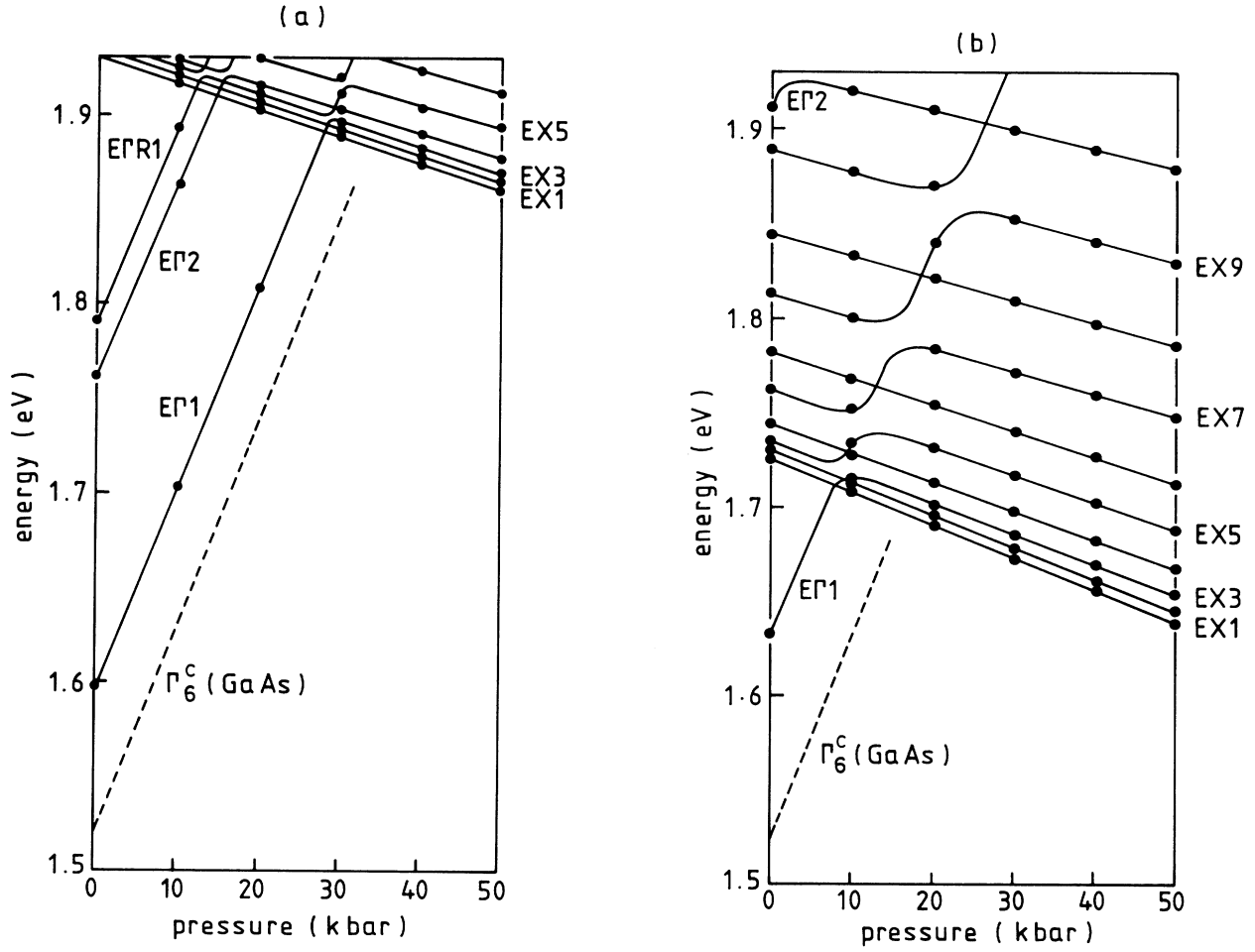

FIG. 11. Variation with hydrostatic pressure of the energies of the lowest conduction states, at the center of the superlattice Brillouin zone, in the (GaAs,51 Å/$Al_xGa_{1-x}As$,102 Å) superlattice with 60:40 offsets with (a) $x=0.25$ and (b) $x=1.0$. The solid dots correspond to the results of full calculations; the solid lines are a guide for the eye. The variation in energy of the edge of the conduction band at Γ_6^c of GaAs is also shown.

TABLE IV. Table giving pressure coefficients for various states shown in Fig. 11 for the (GaAs,51 Å/$Al_xGa_{1-x}As$,102 Å) (001) superlattice. Pressure coefficients for the GaAs (host crystal) Γ_6^c, X_6^c levels are also shown together with the corresponding levels calculated (by exchanging monolayers of GaAs with monolayers of AlAs) for AlAs.

System	Level or state	Pressure coefficient (meV/kbar)
Bulk GaAs	Γ_6^c	10.6
	X_6^c	−1.3
Bulk AlAs	Γ_6^c	10.2
	X_6^c	−1.7
Superlattice; $x=0.25$	EΓ1	10.5
	EΓ2	10.2
	EΓR1	10.4
	EX1	−1.4
Superlattice; $x=1.0$	EΓ1	10.4
	EX1	−1.7
	EX3	−1.6
	EX5	−1.5
	EX7	−1.3

sure coefficients dE/dP for the principal superlattice states shown in Fig. 11. The pressure coefficients of the bulk Γ_6^c and X_6^c levels both of GaAs and $Al_xGa_{1-x}As$ are also given. In the case of $Al_xGa_{1-x}As$, the pressure coefficients which have been given are those which are "seen" in the calculation and are therefore the pressure coefficients which should be compared with those of the superlattice states. Although a convergence problem exists for the lowest X-related states for the case of 60:40 offsets (see earlier discussion) when GaAs is used as the host crystal, it is possible to avoid the problem by choosing AlAs (or $Al_xGa_{1-x}As$) as the host crystal. Of course, the convergence problem would then shift to the Γ (GaAs)-related states. It should be noted, however, that states are trapped in the camel's back near X and so the necessary correction in Figs. 11(a) and 11(b) ($47x$ meV) to the energy of the lowest X-related state in the alloy layer is straightforward.

The most striking feature of Fig. 11 is that, apart from the anticrossing regions, the energy of all states responds more or less linearly with HP. The pressure coefficient of the lowest Γ-related bound state EΓ1 is less than the corresponding coefficient for the Γ_6^c level. This can be explained by the increase in m^* with increasing HP. By comparing Fig. 11 with Fig. 5, it can be seen that some of the effects of HP are very similar to those of alloying. The most striking similarities are of course those in which the energy of particular states change linearly with increasing alloy composition x or increasing HP. For example, it can be seen from Fig. 5 that (i) the energy of state EΓR1 increases linearly with increasing x (for $x \gtrsim 0.2$) and (ii) the energy of state EX1 decreases linearly with increasing x. Other features such as anticrossing of states can also arise as a result either of alloying or of HP. However, a feature which appears to be unique to alloying is the leveling off of an energy level, e.g., that of EΓ1, with increasing x. No such features have been observed in this superlattice with HP increasing from 0 up to 50 kbar.

It is clear from the results presented in Sec. III B that alloying can be used to achieve Γ-X mixing. The same effect can also be achieved with the use of HP. To illustrate this, we show in Fig. 12 the leading coefficients in the spectral distributions of the lowest conduction states in the (GaAs,51 Å/$Al_{0.25}Ga_{0.75}As$,102 Å) superlattice with 60:40 offsets and HP of (a) 0, (b) 10, and (c) 30 kbar. Figure 12(a) shows mixing between EΓR2 and EX1 and comparison with Fig. 6 shows that the spectral distribution of state EΓR1 has evolved into just one peak centered on Γ. As HP is increased from zero pressure, the Γ-related states move up in energy and the X-related states move down in energy. This is reflected not only in Fig. 11(a) but also in the sequence of spectral distributions given in Fig. 12. It can be seen from Fig. 12(c) that state EΓ1 at 30 kbar mixes strongly with state EX5.

In Fig. 13(a), we show the variation with HP of the energy levels of the states at the center of the SBZ in the (GaAs,51 Å/AlAs,6 Å) (001) superlattice with 60:40 offsets. The calculations have been performed using GaAs Bloch states in the expansion of Ψ. The state with the lowest energy at zero pressure is the ground Γ (GaAs)-related state EΓ1 whilst state EX1 directly above it in energy is an X-related state, confined mostly in the AlAs layer. The charge densities of the lowest conduction states at 0 kbar, plotted along a line in the [001] direction

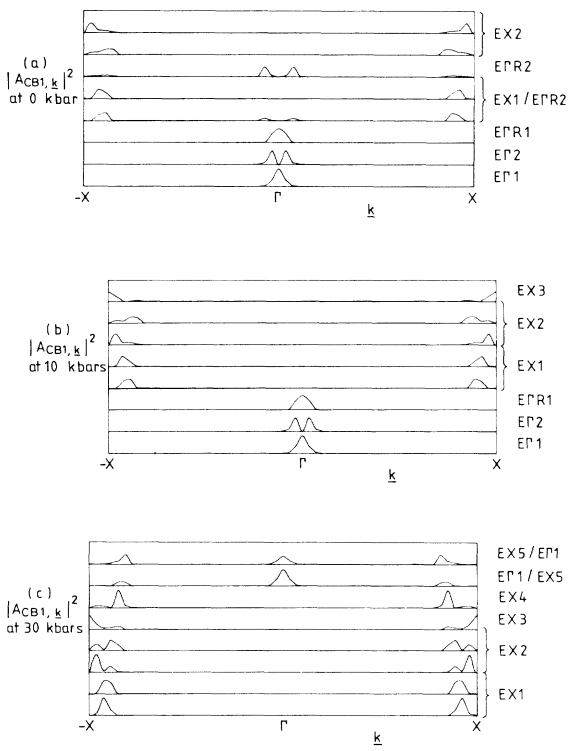

FIG. 12. Plots of $|A_{nks}|^2$ as a function of k_z along the Δ line of the GaAs Brillouin zone for the lowest conduction states, at the center of the superlattice Brillouin zone, in the (GaAs,51 Å/$Al_{0.25}Ga_{0.75}As$,102 Å) superlattice with 60:40 offsets at (a) 0, (b) 10, and (c) 30 kbar. Only contributions from the lowest conduction band have been shown.

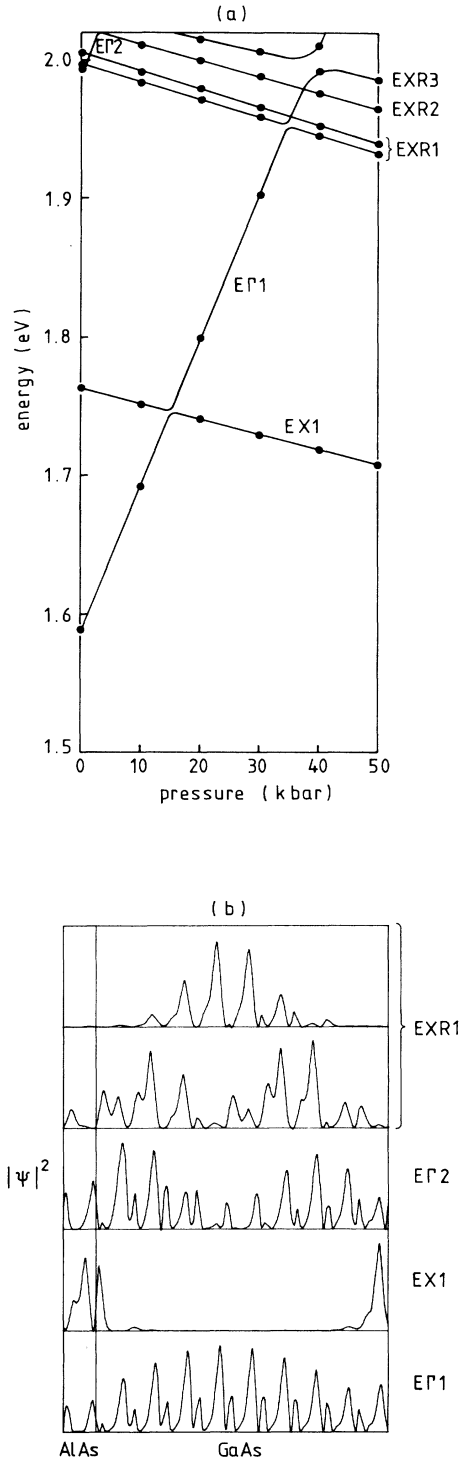

FIG. 13. (a) Variation with hydrostatic pressure of the energies of the lowest conduction states, at the center of the superlattice Brillouin zone, in the (GaAs,51 Å/AlAs,6 Å) superlattice. (b) Charge densities, plotted along the superlattice axis in the [001] direction, of the lowest conduction states from (a) at 0 kbar.

which passes through mid-bond positions, are shown in Fig. 13(b). Since the charge densities, especially those of the X-related states are fairly delocalized around the atomic positions, this figure should only be used to give an indication of the spatial location of the different states. Unlike the bonding states at the top of the valence band, the antibonding states in the conduction band do not have their charge strongly concentrated on the bonds. The reader is referred to Refs. 47 and 48 for charge-density plots and further discussion of spatial localization of charge in bulk states at the edges of bands and to Ref. 8 for a discussion of charge densities in $GaAs/Al_xGa_{1-x}As$ (001) superlattices.

Since the AlAs layer is only two monolayers (6 Å) in width, it cannot be considered to be bulklike. This is because the monolayer on either side of each of the AlAs monolayers is different: on one side is a monolayer of GaAs and on the other side is a monolayer of AlAs. In Fig. 14, we show the dispersion in the k_z direction of the lowest conduction states at (a) 0, (b) 10, and (c) 20 kbar. The dashed curves in Fig. 14(a) show the corresponding dispersions obtained by using AlAs Bloch states in the expansion of Ψ. From Table III, it is reasonable to expect the dashed curves for states EΓ1 and EΓ2 to lie approximately 50 meV above the corresponding solid curves. However, the dashed curve for state EX1 also lies above its corresponding solid curve although on the basis of the data in Table III, one might expect the use of AlAs Bloch states as the basis set to result in a lowering of the energy of state EX1. Since the opposite effect occurs, it must be concluded that strong interaction occurs between the GaAs and the (quasi)-AlAs states in the formation of EX1. In effect, the form of the AlAs band structure which is seen by the superlattice system must be incomplete or at least rather distorted. It has been shown that at least three monolayers of AlAs are required in order to provide sufficient information about the band structure of AlAs near X for a superlattice state to be trapped within the camel's back.[8] For an AlAs layer comprising only three monolayers, it is probably only the middle monolayer which is characteristic of AlAs. Several pseudopotential studies have indicated that disturbances such as charge redistribution between two adjoining semiconductor materials occur in a very narrow region at the interface (e.g., Refs. 49 and 50). It has been shown that the Δ_5 minimum of AlAs lies well below (250–300 meV) the Δ_5 minimum of GaAs for systems in which the AlAs layers are at least 15 Å in width.[8,9] However, the band offsets in systems in which at least one of the layers is only one or two monolayers in width is not known. Until the mechanism(s) which control the band offsets is fully understood, there seems no reason to expect *a fortiori* that the offset (if such a concept still applies) in, say, a (GaAs,51 Å/AlAs,6 Å) superlattice is the same as that in a (GaAs,6 Å/AlAs,51 Å) superlattice. Bearing this in mind, it is clear from Figs. 13 and 14 that the uncertainty can be resolved by appropriate measurements under hydrostatic pressure. Any significant changes in the offset compared with that present in systems with layers of width greater than about 15 Å will result in significant changes in the energy level of state EX1. Experimental

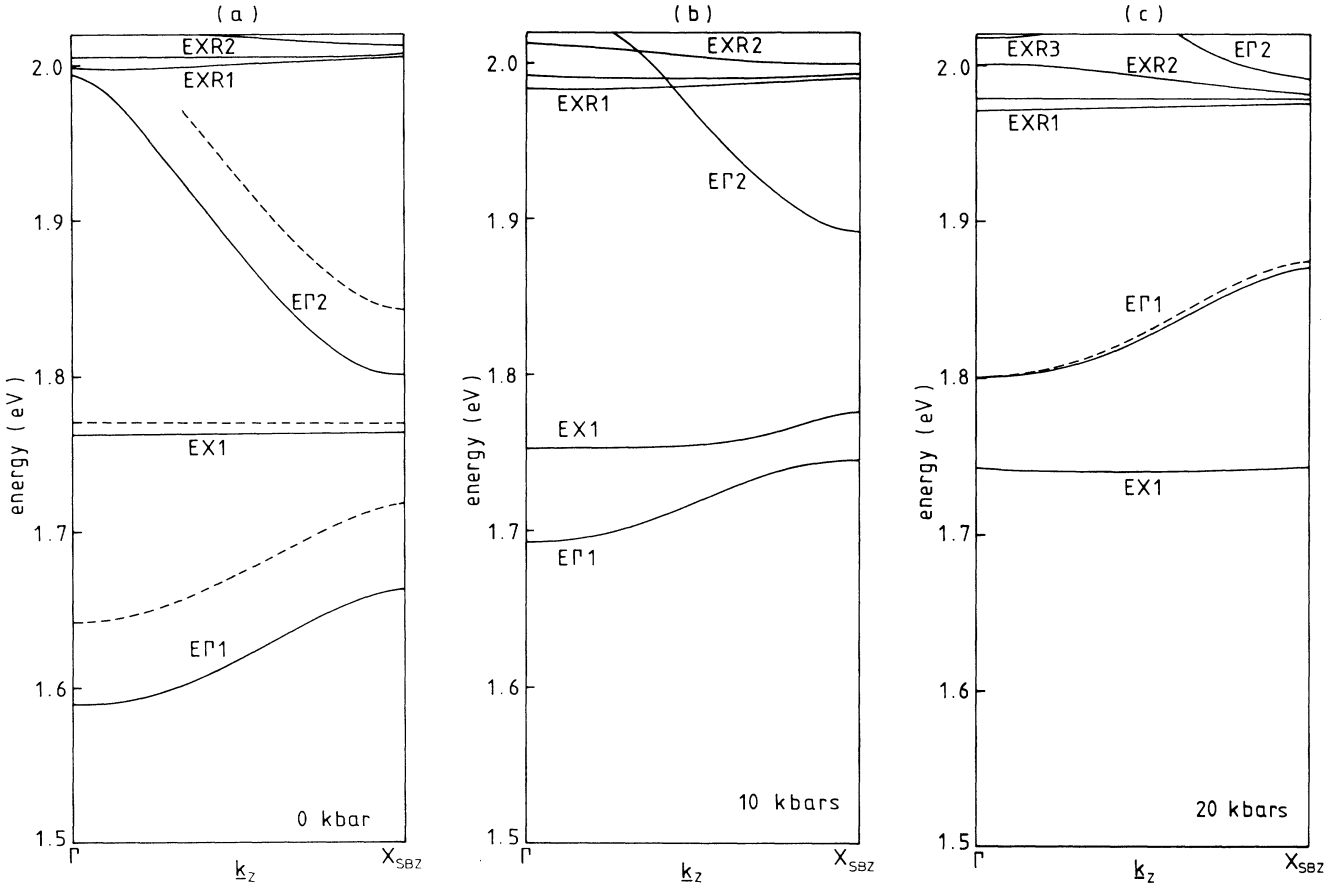

FIG. 14. Dispersions along the Δ_Z line between Γ and X_{SBZ} in the superlattice Brillouin zone of the lowest conduction states in the (GaAs,51 Å/AlAs,6 Å) superlattice with 60:40 offsets at (a) 0, (b) 10, and (c) 20 kbar. The solid curves have been obtained using an expansion of Ψ in terms of GaAs Bloch states. Corresponding curves obtained using AlAs Bloch states are shown dashed in (a) for comparison. The dispersion curve of state EΓ1 at 0 kbar (shown dashed) has been superimposed on the corresponding curve in (c).

determination of the precise energy of the lowest X-related state confined in the AlAs layer will provide important information for the understanding of the physical mechanism(s) which control band discontinuities.

In Fig. 14(c), the dispersion curve of state EΓ1 at 0 kbar (dashed curve) has been superimposed on the corresponding curve at 20 kbar. It can be seen that the width of the subband decreases with increasing HP. This decrease in subband width arises because (i) the curvature of the bulk bands around Γ decreases and (ii) interactions between state EΓ1 and X-related states increase as state EΓ1 moves up in energy. Detailed experimental investigation of the curvatures and widths of these subbands should provide useful information about the deformation of the $E(\mathbf{k})$ surface with HP.

Optical matrix elements at the center of the SBZ for transitions from the ground heavy-hole-like (HH1) state to the lowest conduction states in the (GaAs,51 Å/AlAs,102 Å) superlattice have been calculated. For a given optical polarization, we use the modulus squared of the optical matrix element (M_{if}) for the transition from the initial state i=HH1 to the final state $f=E\Gamma1$ at 0 kbar as the basic unit. In this paper, only transitions with i=HH1 and f=conduction state will be considered and so, for brevity, the modulus squared of the optical matrix element will be referred to as M_{if} without further specification of state i. We use a prime to indicate that the M_{if} have been divided by $M_{\mathrm{HH1,E\Gamma1}}$ (0 kbar). In Fig. 15, we have plotted $\log_{10}(M'_{if})$ against energy level for the lowest conduction states at 0, 10, 20, 30, and 40 kbar. The momentum operator $\hat{\mathbf{P}}$ has been chosen to lie in the [110] direction and logarithms have been plotted to facilitate presentation of the M'_{if}. The points in Fig. 15 which correspond to the ground Γ-related state EΓ1 are labeled. All other points correspond to X-related states which, unlike state EΓ1, are confined in the AlAs layers. The energies of the states as a function of HP have already been shown in Fig. 11(b) and the spectral distributions at 0 kbar have been given in Fig. 7(a). In Fig. 16, we show (a) the spectral distributions and (b) the charge densities of the lowest conduction states at 10 kbar. It is clear from Fig. 16 and Fig. 11(b) that strong mixing (anticrossing) occurs between states EΓ1 and EX5.

It can be seen from Fig. 15 that, for this superlattice, the M_{if} for the transitions between HH1 and the EXn alternate with n such that the largest M_{if} are obtained for

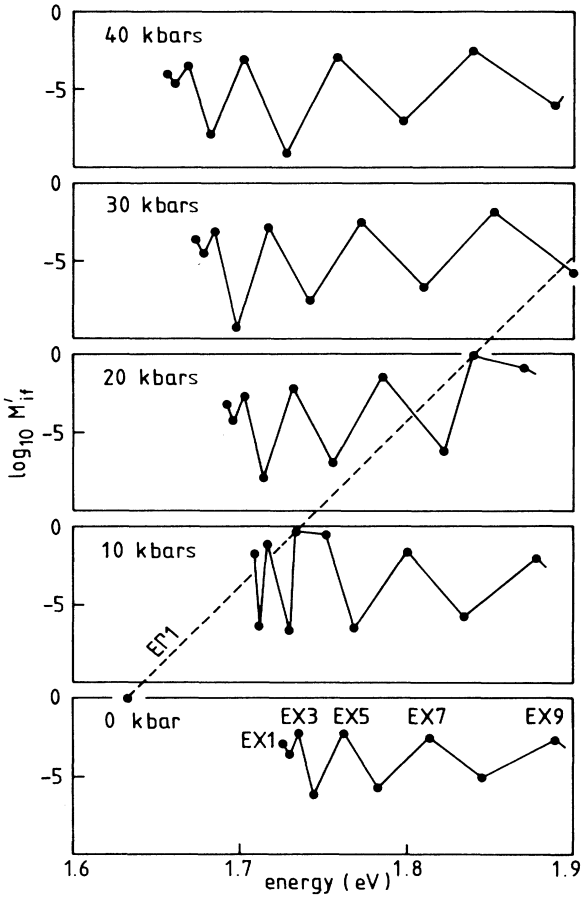

FIG. 15. Plots of $\log_{10}$ of the squared optical matrix element M'_{if} against energy level for the lowest conduction states, at the center of the superlattice Brillouin zone, in the (GaAs,51 Å/AlAs,102 Å) superlattice with 60:40 offsets for hydrostatic pressures ranging from 0 to 40 kbar. The initial state i is the ground heavy-hole-like state (see text). The position of the zone-center-related state EΓ1 has been marked; all other states are zone-edge-related states. The polarization vector $\hat{\mathbf{P}}$ has been chosen to lie in the [110] direction.

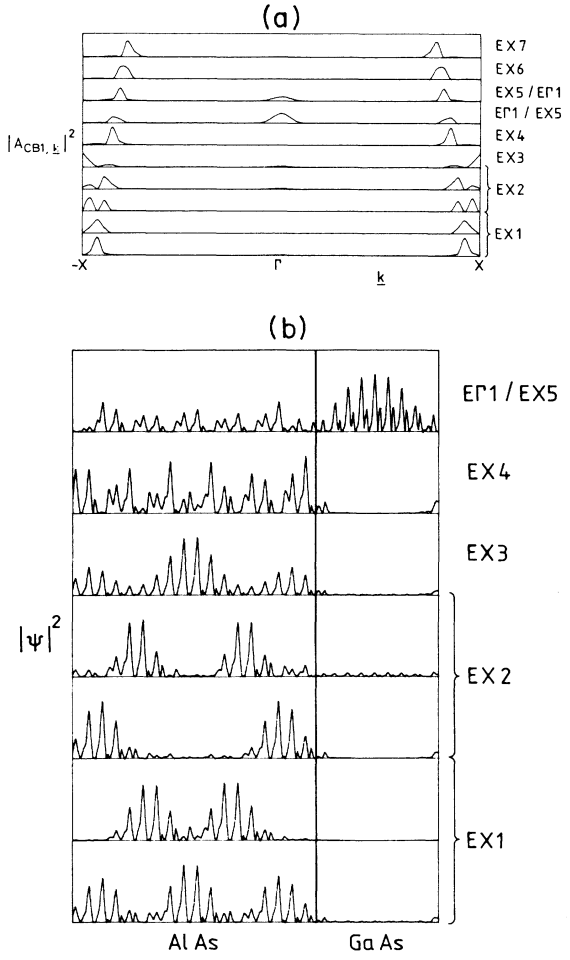

FIG. 16. (a) Plots of $|A_{nks}|^2$ as a function of k_z along the Δ line of the GaAs Brillouin zone for the lowest conduction states, at the center of the superlattice Brillouin zone, in the (GaAs,51 Å/AlAs,102 Å) superlattice with 60:40 offsets at 10 kbar. Only contributions from the lowest bulk conduction band have been shown. (b) Charge densities, plotted along the superlattice axis in the [001] direction of the lowest states from (a).

odd n. It is also evident from Fig. 15 that the M_{if} for the X-related states increase as these states are crossed by the Γ-related state. The lowest M_{if} for the X-related states occur at 40 kbar. However, even at 40 kbar the M_{if} for the EXn (n odd) are between only two and four orders of magnitude smaller than the M_{if} for the transition HH1 to EΓ1 at zero pressure. This would indicate that transitions between the top valence state and various confined states associated with the secondary minima should be measurable. This is in spite of the fact that such transitions must occur across the heterointerface. Of course, no information about the line shape of the HH1-EXn transitions can be obtained from just the M_{if} at the center of the SBZ. In this paper, however, we shall concentrate only on the prediction that transitions such as these should in principle be observable. We shall investigate some of the physics which lies behind our predictions and shall discuss some of the implications.

Since several approximations are made in our calculations, it is necessary to show that the $\log_{10}(M'_{if})$ which have been plotted in Fig. 15 are not fictitious. The most notable approximations are those made in the construction of the potentials with which the calculations are performed. For a given HP, the symmetric and antisymmetric form factors for GaAs and AlAs at the bulk RLV's are fixed (see Table I) but the interpolation of the potential between these Fourier components is arbitrary. Since we use a virtual crystal approximation in order to achieve a rigid shift of one bulk band structure with respect to the other, the value of the symmetric Fourier component of the local potential $V_L^s(q)$ at $q=0$ is also fixed. In Fig. 17(a), we show the curve fitted to the fixed Fourier components of $V_L^s(q)$ at 20 kbar which is used in the calculations. The full curve has been obtained by Lagrange interpolation with the section $12<q^2<16$ scaled down by a factor of 3. The curve in Fig. 17(a) cor-

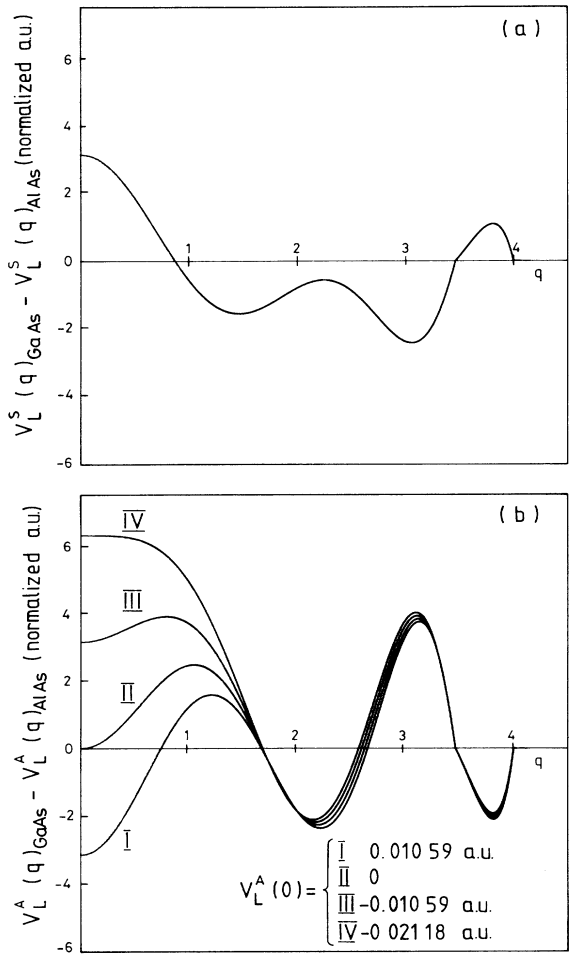

FIG. 17. Plots of (a) the symmetric local potential $V_L^S(q)$ and (b) four different antisymmetric local potentials $V_L^A(q)$ as a function of q for the case of 60:40 offsets at 20 kbar. The potentials are plotted in atomic units normalized to unit volume and q is in units of $2\pi/A$. The four sets of energy levels and squared optical matrix elements which can be obtained with these potentials are shown in Fig. 18. Truncation of the potential at $q^2=12$ makes little difference to the results shown in Fig. 18.

responds to the case of 60:40 offsets.

At $q=0$, the structure factor [cf. Eq. (12)] eliminates the antisymmetric component of the local potential $V_L^A(q)$ and so $V_L^A(0)$ does not affect the band offset. Also, the spin-orbit coupling terms at $q=0$ do not affect the band offset since they involve a vector crossproduct. The value of $V_L^A(0)$, unlike that of $V_L^S(0)$, is therefore arbitrary. In Fig. 17(b), we show four curves for the antisymmetric local potential $V_L^A(q)$ at 20 kbar which have been obtained by arbitrarily fixing $V_L^A(0)$ at values of $-0.021\,18$, $-0.010\,59$, 0, and $0.010\,59$ a.u. (normalized to unit volume). We note that the four curves are not only different at and near $q=0$ but also differ slightly at the larger values of q except exactly at the bulk RLV's.

Although the use of the curve in Fig. 17(a) with any of the curves in Fig. 17(b) can be used to simulate a GaAs/AlAs superlattice with 60:40 offsets, long-wavelength (small q) scattering processes in the four possible calculations will be very different. Unless otherwise specified, the results of all calculations which are presented in this paper have been obtained using a curve for $V_L^A(q)$ in which $V_L^A(0)$ has been set to zero.

In Fig. 18, we show $\log_{10}(M'_{if})$ plotted against energy for the lowest conduction states in the (GaAs,51 Å/AlAs,102 Å) superlattice at 20 kbar obtained using the four possible combinations of the potentials shown in Fig. 17. The results in Fig. 18 which correspond to the case with $V_L^A(0)=0$ are the same as those which have already been presented in Fig. 15. M_{if}, for the transition between HH1 and EΓ1 at 0 kbar in the calculation with $V_L^A(0)=0$ has been used as the basic unit. We have chosen to test the effects of the variation in the long-wavelength scattering processes for the case of 20 kbar since, at this pressure, state EΓ1 sits amongst and is strongly mixed with the X-related states. The calculations therefore represent a very difficult test of the small-q approximations in the potentials.

It can be seen from Fig. 18 that the largest variations in M_{if} are those associated with the EXn (n even). However, apart from M_{if} for EX1, which varies by only one order of magnitude, the M_{if} for EXn (n odd) and especially EΓ1 hardly change. We therefore conclude that uncertainties in the long-wavelength components of our potential cannot qualitatively affect our predictions about the observability of HH1-EXn transitions. It should also be noted that the largest variation in energy shown in Fig. 18 is only 10 meV (see state EX9/EΓ1). Results similar to those shown in Fig. 17 (at 20 kbar) are also obtained with a potential in which all Fourier components with $q^2>12$ are set to zero.

It was mentioned earlier how removal of the camel's backs near X resulted in the breaking of the quasidegen-

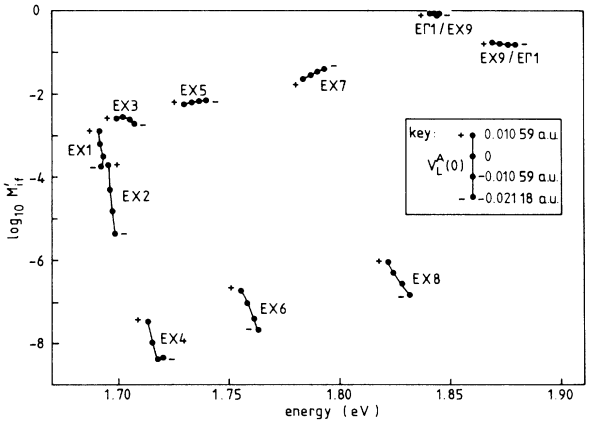

FIG. 18. Plots of $\log_{10}$ of the squared optical matrix element M'_{if} against energy level for the lowest conduction states, at the center of the superlattice Brillouin zone, in the (GaAs,51 Å/AlAs,102 Å) superlattice with 60:40 offsets at 20 kbar. The four results shown for each state correspond to results obtained with the four different antisymmetric local potentials $V_L^A(q)$ shown in Fig. 17(b).

eracies amongst the lowest X-related states. The camel's back is not responsible either for the large M_{if} which are calculated for transitions between the ground heavy-hole-like state and the zone-edge-related states. In order to demonstrate this, we have recalculated the M_{if} for the (GaAs,51 Å/AlAs,102 Å) superlattice at 20 kbar [see Fig. 19(c)] having artificially removed the camel's back from the band structure of the host crystal. The results obtained using the unadjusted host-crystal band structure are shown again in Fig. 19(a) for direct comparison. The downward pointing arrows in Fig. 19 indicate states which are quasi-doubly degenerate. Although the ground Γ-related state EΓ1 has been labeled, its precise energy in Fig. 19(c) is not significant since the results depend on the curvature of the imposed band structure. By comparing Fig. 19(a) with Fig. 19(c), we can see that the number (10) of superlattice states in the energy range considered is the same and that removal of the camel's back near X has made little difference to the optical matrix elements.

In order to demonstrate that observable transitions between the ground heavy-hole-like state and the X-related states are not a peculiarity of the (GaAs,51 Å/AlAs,102 Å) system, we consider two more different superlattices. In Fig. 19(b), we show the $\log_{10}M'_{if}$ against energy level for the lowest conduction states in the (GaAs,51 Å/AlAs,232 Å) superlattice at 20 kbar with 60:40 offsets. By comparing Fig. 19(a) with 19(b), it can be seen that although the widening of the AlAs layer has resulted in the creation of additional X-related states, the alternation of large and small M_{if} is retained. It is still the EXn (n odd) which have the largest M_{if}. In Fig. 20, we compare the

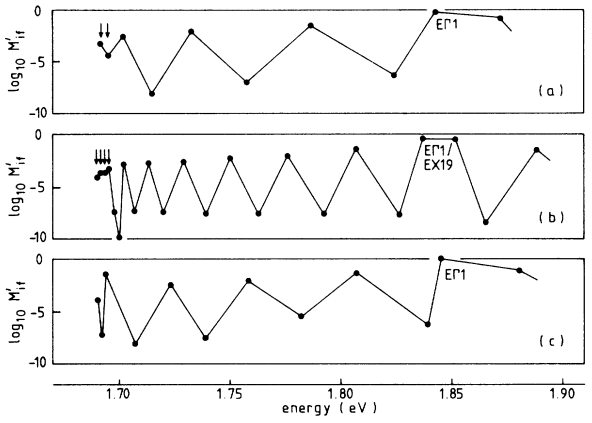

FIG. 19. Plot of $\log_{10}$ of the squared optical matrix element M'_{if} against energy level for the lowest conduction states, at the center of the superlattice Brillouin zone, in (a) the (GaAs,51 Å/AlAs,102 Å) superlattice, (b) the (GaAs,51 Å/AlAs,232 Å) superlattice, and (c) the (GaAs,51 Å/AlAs,102 Å) superlattice. All three sets of results have been obtained with 60:40 offsets at 20 kbar. The results in (a), shown here for direct comparison, have already been shown in Fig. 15. The results in (c) correspond to the case in which the camel's backs in the host-crystal (GaAs) band structure have been artificially removed. The downward pointing arrows indicate pairs of quasidegenerate zone-edge-related states. The polarization vector $\hat{\mathbf{P}}$ has been chosen to lie in the [110] direction.

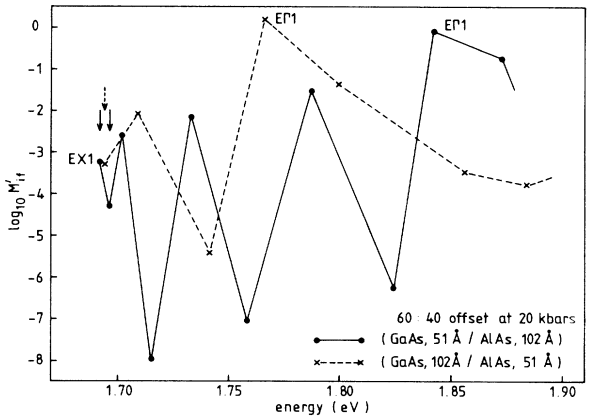

FIG. 20. Plots of $\log_{10}$ of the squared optical matrix element M'_{if} against energy level for the lowest conduction states, at the center of the superlattice Brillouin zone, in the (GaAs,51 Å/AlAs,102 Å) and (GaAs,102 Å/AlAs,51 Å) superlattices with 60:40 offsets at 20 kbar. The downward pointing arrows indicate pairs of quasidegenerate zone-edge-related states. The polarization vector $\hat{\mathbf{P}}$ has been chosen to lie in the [110] direction.

$\log_{10}M'_{if}$ against the energy level for the transition between HH1 and the lowest conduction states in the (GaAs,51 Å/AlAs,102 Å) and (GaAs,102 Å/AlAs,51 Å) superlattices at 20 kbar with 60:40 offsets. The only Γ-related state shown for each of these superlattices is the ground Γ (GaAs)-related state EΓ1. All other states are X(AlAs)-related states and those which are quasi-doubly degenerate have been indicated with a downward pointing arrow. The points corresponding to the (GaAs,102 Å/AlAs,51 Å) superlattice show that some HH1-EXn transitions should be observable with [110] polarized light. However, the M_{if} in the sequence of EXn do not alternate compared with those for the (GaAs,51 Å/AlAs,102 Å) superlattice. This is because the increased width of the GaAs layer has resulted in a closer spacing of the Γ (GaAs)-related states and so Γ-X interactions are complicated by remnant Γ components in the wave functions of the EXn.

In Table V, we show values of $\log_{10}M'_{if}$ for the transitions between the ground heavy-hole-like state HH1 and the lowest conduction states in the (GaAs,51 Å/AlAs,102 Å) superlattice at 20 kbar with 60:40 offsets. The values in column (a) are again those which have been plotted in Fig. 15. These M_{if} were calculated using an expansion of Ψ in terms of GaAs Bloch states from the four bulk bands, VB2, VB3, VB4, and CB1. In column (b), we show the $\log_{10}M'_{if}$ which are obtained when the $A_{n\mathbf{k}s}$ in the superlattice wave functions for $|\mathbf{k}_z| > 0.152\pi/A$ are set to zero and so the only nonzero components in the wave functions are those in the region of the zone center. Since there is little difference between the values in column (a) and those in column (b), we conclude that enhancement of the M_{if} for the EXn is a direct result of the introduction of zone-center components into the wave functions.

Since our diagonalization procedure incorporates an orthonormalization routine, M_{if} for transitions between, say, HH1 and conduction states can be calculated using

TABLE V. Table showing values of $\log_{10}M'_{if}$ for the transitions between HH1 and the lowest conduction states in the (GaAs,51 Å/AlAs,102 Å) superlattice at 20 kbar with 60:40 offsets. The values in column (a) are those which have been plotted in Fig. 15. These M'_{if} were calculated using an expansion of ψ in terms of GaAs Bloch states from the four bulk bands VB2, VB3, VB4, and CB1. The $\log_{10}M'_{if}$ in column (b) were obtained after retaining only zone-center components (see text) in the wave functions of the states. The $\log_{10}M'_{if}$ in columns (c) and (d) were obtained using the approximation of decoupled valence and conduction bands (see text) with a full-zone expansion of the conduction states in terms of (c) CB1 and (d) CB1 and CB2.

State	(a)	(b)	(c)	(d)
EX1	−3.218	−3.222	−3.176	−3.306
EX2	−4.305	−4.306	−5.239	−5.825
EX3	−2.567	−2.571	−2.541	−2.598
EX4	−7.991	−7.167	−6.101	−8.414
EX5	−2.202	−2.206	−2.193	−2.221
EX6	−7.043	−7.163	−6.240	−7.153
EX7	−1.539	−1.542	−1.542	−1.542
EX8	−6.294	−7.877	−6.536	−6.318
EΓ1 (EX9)	−0.079	−0.079	−0.091	−0.078
EX9 (EΓ1)	−0.786	−0.785	−0.723	−0.778

superlattice pseudofunctions which have been obtained from separate calculations of the electronic structure of the valence and conduction bands. Since the valence and conduction bands are totally decoupled in such calculations, the approximation makes sense only for superlattices in which the layers are reasonably thick ($\gtrsim$50 Å). To justify this, we show in Table V [columns (c) and (d)] $\log_{10}M'_{if}$, calculated using the approximation of decoupled valence and conduction bands. The numbers in column (c) and column (d) have been obtained using superlattice valence states expanded in terms of VB2, VB3, and VB4 with $\mathbf{k}$ restricted to the third of the BBZ centered on Γ. In the case of the $\log_{10}M'_{if}$ shown in column (c), the superlattice conduction states Ψ_c were obtained with a full-zone expansion only in terms of states from the lowest bulk conduction band CB1. The corresponding numbers shown in column (d) were obtained with Ψ_c expanded in terms of Bloch states from the two lowest conduction bands, CB1 and CB2. Although no significant differences in energy ($\lesssim$5 meV) were obtained for the states in Table V in the three separate calculations (a), (c), and (d), the introduction of CB2 into the expansion of Ψ_c in (d) does cause a systematic lowering in energy of all the CB states, as would be expected within the framework of perturbation theory. By comparing the numbers in columns (a), (c), and (d) of Table V, it can be seen that there is little variation in the $\log_{10}M'_{if}$ for the three cases. This confirms the validity of the approximation of VB-CB decoupling for this width of layer at least for the M_{if} associated with transitions across the superlattice gap from HH1. This approximation is used throughout the paper for superlattices with alloy widths greater than 102 Å. The numbers in Table V also justify the expansion of Ψ_c in terms of only CB1, at least for those states within about 450 meV from the conduction band edge of GaAs for the case of 60:40 offsets.

IV. MQWS's: RESULTS AND DISCUSSION

We turn our attention to systems in which the width of the GaAs layer (51/102 Å) is small compared with that (514 Å) of the AlAs layer. These systems can in effect be considered as multiquantum well structures (MQWS's) since the AlAs (barrier) layer is sufficiently thick to inhibit significant penetration by the states confined in the GaAs layers. Within our pseudopotential scheme, however, these MQWS's are still strictly superlattices since numerical implementation of the scheme rests on the property of periodicity. We shall focus predominately on the variation with HP of the electronic and optical properties of the (GaAs,51 Å/AlAs,514 Å) and the (GaAs,102 Å/AlAs, 514 Å) MQWS's with 85:15 offsets since these systems can be used to study various Γ-X crossings which are not obscured by the presence of a multitude of extended bulklike (AlAs) zone-edge states, as in the case of 60:40 offsets. We shall show, however, that the effects observed with 85:15 offsets are conceptually and in some respects almost quantitatively no different from those observed with 60:40 offsets.

In Fig. 21(a), we show the moduli squared of the $A_{n\mathbf{k}s}$ coefficients near Γ_6^c for the four lowest zone-center-related conduction states EΓ1—EΓ4 at the center of the SBZ in the (GaAs,102 Å/AlAs,514 Å) MQWS at 0 kbar. These zone-center-related states are confined in the GaAs layers. Owing to the size of the period, various limitations are placed on the expansions of the superlattice wave functions. The approximation of decoupled valence and conduction bands is used. For the conduction states, we use a full-zone, one-band (CB1) approximation and for the valence states we use a partial-zone ($\frac{1}{3}$ of BBZ centered on Γ), multi-band (VB2, VB3, and VB4) approximation. On account of these approximations, we are, as mentioned earlier, restricted to those states lying within 450—550 meV from the band edges. This energy range corresponds to the two cases of band offset (60:40 and 85:15) which are considered in this study.

The spectral distributions in Fig. 21(a) have been shown in order to highlight a general feature of the zone-center-related states in the MQWS's. The EΓn states with n odd have a peak in their spectral distributions at Γ_6^c whilst the EΓn states with n even do not. Bearing in mind that only

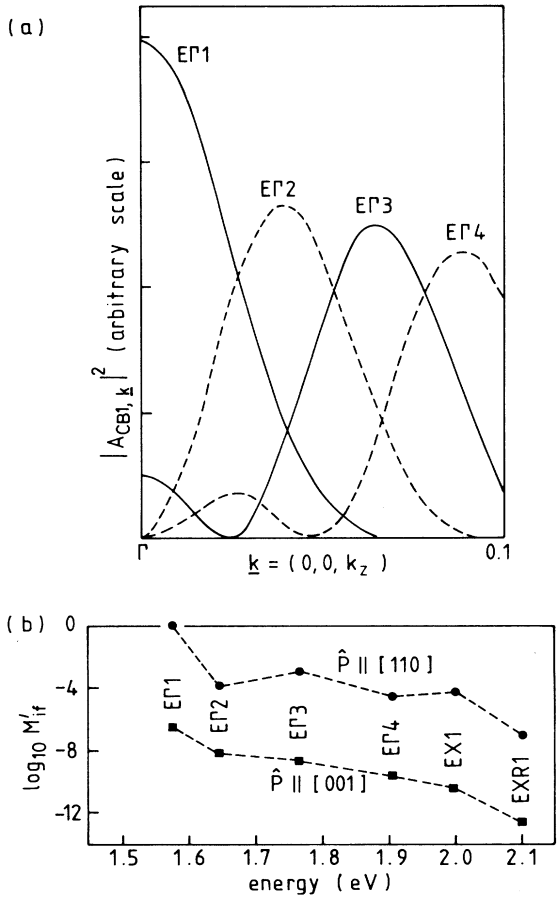

FIG. 21. (a) Plot of $|A_{nks}|^2$ as a function of $\mathbf{k}_z$ along the Δ line of the GaAs Brillouin zone between Γ and $\mathbf{k}=(0,0,0.1)2\pi/A$ for the lowest four zone-center-related states, at the center of the superlattice Brillouin zone, in the (GaAs,102 Å/AlAs,514 Å) MQWS with 85:15 offsets at 0 kbar. Only contributions from the lowest bulk conduction band have been shown. (b) Plot of $\log_{10}$ of the squared optical matrix element M'_{if} against energy level for the lowest six states, at the center of the superlattice Brillouin zone, in the (GaAs,102 Å/AlAs,514 Å) MQWS with 60:40 offsets at 0 kbar. Two cases of optical polarization have been shown.

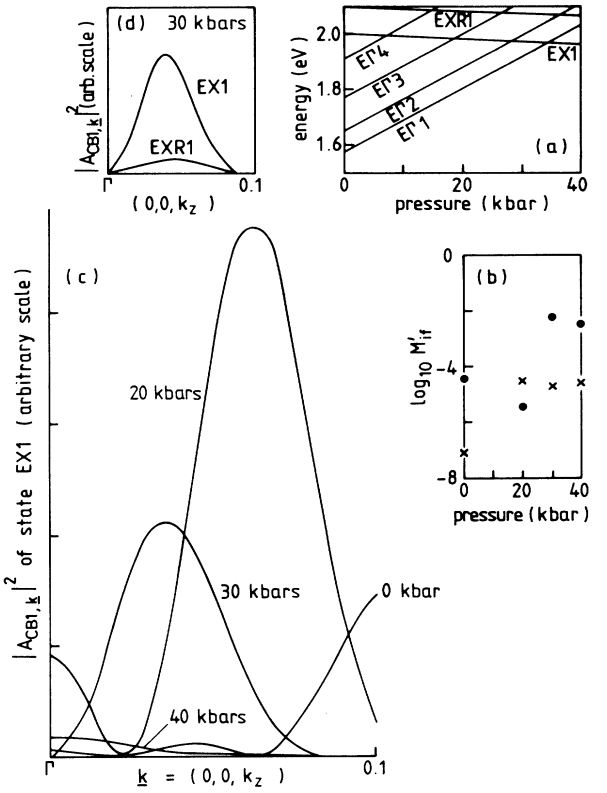

FIG. 22. Results concerning the lowest conduction states, at the center of the superlattice Brillouin zone, in the (GaAs,102 Å/AlAs,514 Å) MQWS with 85:15 offsets. (a) Energies calculated as a function of hydrostatic pressure. (b) Plot of $\log_{10}$ of the squared optical matrix element M'_{if} with [110] polarization against hydrostatic pressure for states EX1 and EXR1. (c) Plots of $|A_{nks}|^2$ of state EX1 as a function of $\mathbf{k}$ along the Δ line of the GaAs Brillouin zone near Γ at hydrostatic pressures of 0, 20, 30, and 40 kbar. Only contributions from the lowest bulk conduction band have been shown. (d) Plots of $|A_{nks}|^2$ of states EX1 and EXR1 as a function of $\mathbf{k}$ along the Δ line of the GaAs Brillouin zone near Γ at hydrostatic pressure of 30 kbar. Only contributions from the lowest bulk conduction band have been shown.

those A_{nks} weightings lying in the irreducible segment of the BBZ have been included in Fig. 21(a) (the spectral distributions of the states at the center of the SBZ are symmetric with respect to inversion of $\mathbf{k}$), it can be seen that the distributions in wave-vector space of EΓ1—EΓ4 reflect the charge-density distributions in real space.

In Fig. 21(b), we show $\log_{10}M'_{if}$ at 0 kbar for states EΓ1—EΓ4 and states EX1 and EXR1 in the (GaAs,102 Å/AlAs,514 Å) MQWS's. EX1 corresponds to a pair of quasidegenerate states confined in the GaAs layers whilst EXR1 corresponds to a pair of quasidegenerate quasiextended states in the AlAs layers. Before discussing these optical matrix elements, we show in Fig. 22, (a) the variation in energy of states EΓ1—EΓ4, EX1 and EXR1 with HP, (b) the variation of $\log_{10}M'_{if}$ for states EX1 and EXR1 with HP, (c) the zone-center components in the spectral distributions of state EX1 at 0, 20, 30, and 40 kbar, and (d) the zone-center components in the spectral distributions of states EX1 and EXR1 at 30 kbar. Returning to Fig. 21(b), it can be seen that with the polarization vector $\hat{\mathbf{P}}$ lying in the [110] direction, M_{if} for the transitions from HH1 to EΓn alternate with n. This alternation is a reflection of the alternation in the components at and near Γ_6^c which are shown in Fig. 21(a). The $\Delta n=0$ rule (e.g., see Ref. 1) for allowed optical transitions is based on this alternation. It should be noted, however, that the $\log_{10}M'_{if}$ for the EΓn (n even) states indicate that these transitions are weakly allowed. Figure 21(b) also shows that $\log_{10}M'_{if}$ for state EX1 is comparable with that for state EΓ4 and is only four orders of magnitude less than for state EΓ1. This is due to a mixing between state EΓ5 and EX1 which has resulted in the introduction of zone-center components into the wave function of state EX1 at 0 kbar. The $\log_{10}M'_{if}$, which are shown in

Fig. 21(b) for $\hat{\mathbf{P}}$ lying in the [001] direction, correspond to unobservable transitions in the case of all of the states considered.

It can be seen from Fig. 22(a), that as HP is increased the energies of the EΓ states increase linearly and the energies of the EX states decrease linearly. This is similar to the response which has already been shown for the other superlattices. As the EΓ states approach and cross the EX states, Γ-X mixing takes place and zone-center components are introduced into the EX states (and conversely zone-edge components are introduced into the EΓ states). Apart from cases of multiple mixings, the distribution of these zone-center components in the EX states, either those confined in the GaAs layers or those quasiextended in the AlAs layers, reflects the spectral distribution of the particular EΓ state with which interaction is occurring. This is illustrated in Figs. 22(c) and 22(d). The mixing of zone-center components into the EX states is accompanied by an increase in the M_{if}. In 22(c), it can be seen that the M_{if} with $\hat{\mathbf{P}}$ lying in the [110] direction for states EX1 and EXR1 correspond to observable transitions, especially at pressures above about 20 kbar.

In Fig. 23, we show results for the (GaAs,51 Å/AlAs,514 Å) MQWS which are analogous to those shown in Fig. 22. Since there are fewer EΓ states, the situation is less complicated than that illustrated in Fig. 22. The dramatic increase in $\log_{10}M'_{if}$ for state EX1 at 30 kbar [Fig. 23(b)] can be seen to coincide with the EΓ1/EX1 crossing and the dramatic increase in zone-center components in the spectral distribution of state EX1.

In Fig. 24, we compare the spectral distribution of state EΓ1 in (a) the (GaAs,51 Å/AlAs,514 Å) and (c) the (GaAs,102 Å/AlAs,514 Å) MQWS's at 0 kbar. The arrow on each curve in Fig. 24 (and 23) indicates the point at which the modulus squared of the A_{nks} coefficients has dropped to half of the peak height. It can be seen that at 0 kbar, the localization of state EΓ1 in wave-vector space is greater in the case of the 102 Å GaAs layer than in the case of the 51 Å GaAs layer. This is expected from the basic properties of Fourier transforms. As the thickness of the GaAs layer increases to several hundred Å, the layer becomes bulklike and a transition from confined to extended character must take place. In the limit of bulk GaAs, the spectral character of each electronic state must correspond to a highly restricted region of wave vector space centered on a $\mathbf{k}$ point permitted by the dimensions of the crystal.

It can be seen from Fig. 23(b) that M_{if} for EX1 in the (GaAs,51 Å/AlAs,514 Å) MQWS at 0 kbar is only about three orders of magnitude smaller than that for EΓ1. This is in spite of the fact that the moduli squared of the zone-center components in EX1 are considerably smaller than those of EΓ1 [see Fig. 23(c) and compare curves (*a*) and (*b*) in Fig. 24]. In Fig. 24 curve (*d*) we show the zone-center components in the spectral distribution of EΓ1 in the (GaAs,102 Å/AlAs,514 Å) MQWS at 40 kbar. By comparing curve (*c*) with curve (*d*) in Fig. 24, it can be seen that, although EΓ1 at 40 kbar is strongly mixed with zone-edge-related states, the form of the zone-center manifold is unchanged. Over most of the

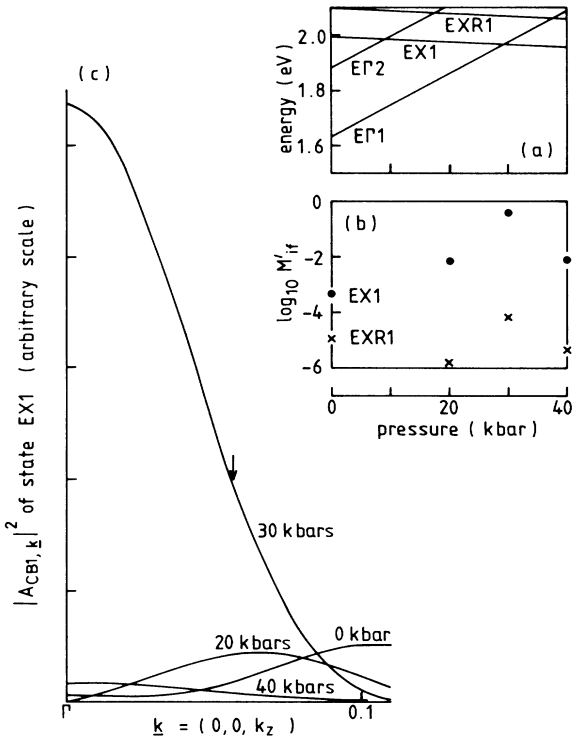

FIG. 23. Results concerning the lowest conduction states, at the center of the superlattice Brillouin zone, in the (GaAs,51 Å/AlAs,514 Å) MQWS with 85:15 offsets. (a) Energies calculated as a function of hydrostatic pressure. (b) Plot of $\log_{10}$ of the squared optical matrix element M'_{if} with [110] polarization against hydrostatic pressure for states EX1 and EXR1. (c) Plots of $|A_{nks}|^2$ of state EX1 as a function of $\mathbf{k}$ along the Δ line of the GaAs Brillouin zone near Γ at hydrostatic pressures of 0, 20, 30, and 40 kbar. Only contributions from the lowest bulk conduction band have been shown.

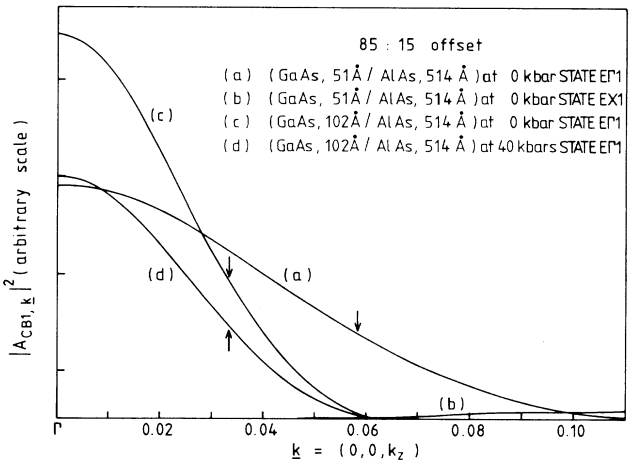

FIG. 24. Plots of $|A_{nks}|^2$ as a function of $\mathbf{k}$ along the Δ line of the GaAs Brillouin zone for various MQWS states, at the center of the appropriate superlattice Brillouin zone. Only contributions from the lowest bulk conduction band have been shown.

wave-vector space shown in Fig. 24, curve (d) can be obtained from curve (c) by linear scaling. Apart from complications due to multiple mixings, similar properties hold for zone-edge components in the spectral distributions.

The results which have been shown in Figs. 21—24 for the (GaAs,51 Å/AlAs,514 Å) and (GaAs,102 Å/AlAs,514 Å) MQWS's correspond to the case of 85:15 offsets. Similar results can be shown for the case of 60:40 offsets although the situation is complicated by the fact that X_6^c (AlAs) lies well below X_6^c (GaAs). Under these circumstances, the lowest confined states in the GaAs layers are meshed between the extended zone-edge states of AlAs and so it is not so easy to disentangle the various Γ-X crossings. In order to highlight this point and to demonstrate that the M_{if} shown in Figs. 21—23 are not peculiar to 85:15 offsets, we have plotted in Fig. 25(a) $\log_{10}M'_{if}$ against energy level for the states at the center of the SBZ in the (GaAs,102 Å/AlAs,514 Å) MQWS at 0 kbar with 60:40 offsets. In Fig. 25(a), three of the states EΓ1, EΓ2, and EΓ3 are confined states localized in the GaAs layers, whilst all of the other states shown are quasicontinuum (extended) zone-edge AlAs states. Apart from the pairs of doubly degenerate zone-edge states lying below X_6^c (AlAs), the zone-edge states are singly degenerate (neglecting spin degeneracy). It can be seen from Fig. 25(a), that the only confined zone-center-related state lying amongst the extended zone-edge states is EΓ3. In Fig. 25(b), we show the modulus squared of the $A_{n\Gamma s}$ component of the states in Fig. 25(a) which lie above state EΓ2. It can be seen From Fig. 25(b) that the interaction between state EΓ3 and the neighboring zone-edge-related states has led to a spreading out of the Γ-point components from state EΓ3. It is evident from Fig. 25(b) and the previous discussion that the movement of a particular

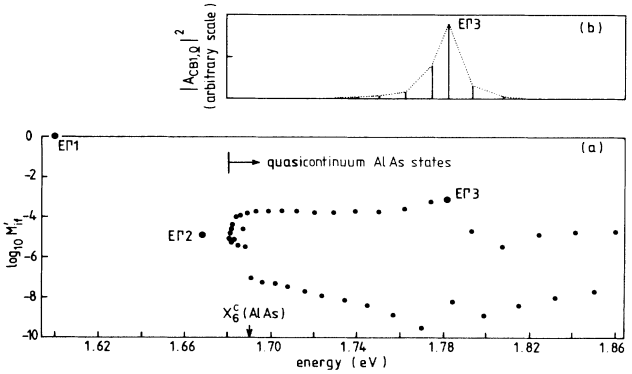

FIG. 25. (a) Plot of $\log_{10}$ of the squared optical matrix element M'_{if} against energy level for the lowest conduction states, at the center of the superlattice Brillouin zone, in the (GaAs,102 Å/AlAs,514 Å) MQWS with 60:40 offsets of 0 kbar. The three zone-center-related states (EΓ1, EΓ2, and EΓ3), confined mostly in the GaAs layers, have been marked. All of the other states which have been shown are zone-edge-related states quasiextended in the AlAs layers. Twelve pairs of quasidegenerate states lie in the camel's backs of AlAs below the energy corresponding to the X_6^c point. (b) Plot of $|A_{n\Gamma s}|^2$ for the states shown in (a) which lie above EΓ2 in energy. The (alternate) zone-edge-related states which have finite A_{nks} at Γ are those which have the largest M_{if}.

state with alloying, HP or changing geometry should be regarded as the movement of a pocket of components in wave-vector space. Interactions between zone-center- and zone-edge-related states (Fig. 25) has given rise to M_{if} for extended AlAs states which correspond to transitions from HH1 across the heterointerface which are in principle observable. The alternation of the M_{if} for the (AlAs) zone-edge-related states [see Fig. 25(a)] is a result of the property of periodicity which is retained within the calculations. If these states were true continuum states, strong Γ-X mixing would not be restricted to alternate states.

V. COMPARISON BETWEEN THEORY AND EXPERIMENT

In order to provide a direct comparison between theory and experiment regarding zone-center—zone-edge mixing, we present in Fig. 26 the calculated and measured pressure dependence of the EΓ1-HH1 and EX1-HH1 transitions for the (GaAs,68 Å/$Al_{0.28}Ga_{0.72}As$,68 Å) (001) superlattice. The details of the experimental method have been given elsewhere.[9] Figure 26 shows that the calculated pressure dependence of the EΓ1-HH1 transition agrees well with the experiment although the slope of the EX1-HH1 transition deviates slightly from the measured one. In our calculations, we have assumed that the pressure coefficients of the Γ and X band gaps of AlAs are the same as those of GaAs (10.6 meV/kbar for the gap at Γ and -1.3 meV/kbar for the gap at X). We have also neglected the possibility of small changes in the band offset and exciton binding energy with pressure as well as dynamic effects at the interfaces reflecting the functional form of the oscillator strength versus pressure. A combined effect of such uncertainties which are not yet fully understood must be responsible for the discrepancy concerning the EX1-HH1 transition. Since the EΓ1 and HH1 states essentially follow the Γ valley of GaAs, the agreement between experiment and theory for the EΓ1-HH1 transition is not surprising. With regard to the EX1-HH1 excitonic transition, we refer the reader to the paper by Bastard *et al.* where a model for excitonic effects in a similar type-II system has been given.[51] At the crossing between the XΓ1-HH1 and EX1-HH1 lines in Fig. 26 which occurs at about 30 kbar, the Γ valley of GaAs and the X valley of $Al_{0.28}Ga_{0.72}As$ are almost degenerate in energy for a band offset of approximately 71:29. The resulting mixing between the zone center and zone-edge components of the corresponding wave functions is reflected in a rapid increase in the oscillator strength $F_{EX1\text{-}HH1}$ of the EX1-HH1 transition. This is clearly shown in Table VI, from which it can be seen that the oscillator strengths for the EΓ1-HH1 and EX1-HH1 transitions are comparable at 30 kbar.

The zone-edge-related state EX1 is localized in the alloy layers and the zone-center-related states EΓ1 and HH1 are localized in the GaAs layers. However, the Γ-x mixing gives rise to a substantial amplitude of state EX1 in the GaAs layers, as shown in Fig. 27(a). In Fig. 27(b), we show the charge remaining in state EX1 after zone-center components have been removed from its wave function. It can be seen that the amplitude in the GaAs layers has

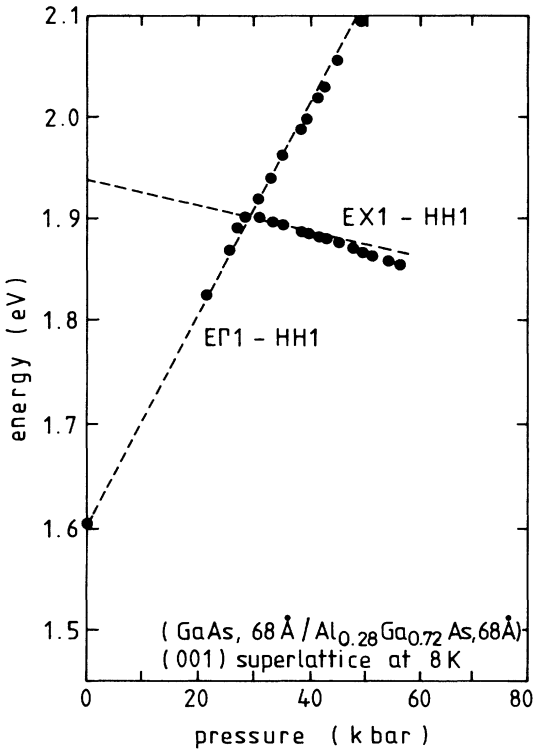

FIG. 26. Photoluminescence (8 K) of a 40-period (GaAs,68 Å/$Al_{0.28}Ga_{0.72}As$,68 Å) (001) superlattice prepared by metalorganic chemical vapor deposition (MOCVD) and held at indicated pressures in a diamond anvil cell. Energies of the Γ-confined transitions (EΓ1-HH1) increase with pressure, following the shift of the direct GaAs band edge, while intensities rapidly diminish near and above 31 kbar. A staggered-band, X-confined transition (EX1-HH1) appears here, and shifts down in energy, weakening with increasing pressure [after Wolford *et al.* (Ref. 9)]. The dashed lines show the corresponding calculated transition energies. The calculations have been performed with a 71:29 offset using the band gaps of GaAs and $Al_xGa_{1-x}As$ at atmospheric pressure given in Ref. 9. It has been assumed that the pressure coefficients of the Γ and X band gaps of $Al_xGa_{1-x}As$ are the same as those which have been measured for GaAs (Ref. 22). An allowance of 20 meV has been made for the indirect exciton. The reader is referred to the paper by Bastard *et al.* (Ref. 51) where a discussion of exciton effects in a type-II structure has been given.

been quenched. We therefore conclude that there is a one-to-one correspondence between localization of and bulk components within the wave functions.

In order to provide more insight into the Γ-X mixing, we present an effective mass model, which in spite of its very restrictive assumptions, reflects all of the key features. Let us assume that the only relevant interaction is between one Γ (zone-center) state and one X (zone-edge) state. Away from the crossing, let the wave functions of the Γ and X states be $\Psi_\Gamma(\mathbf{r})=F_\Gamma(z)\phi_\Gamma(\mathbf{r})$ and $\Psi_X(\mathbf{r})=F_X(z)\phi_X(\mathbf{r})$, where F_Γ, F_X are slowly varying envelopes and ϕ_Γ, ϕ_X are the respective Bloch states. At the crossing, the energies E_Γ and E_X are almost degenerate. In first order perturbation theory, we can write

$$\Psi(\mathbf{r})=C_\Gamma\Psi_\Gamma(\mathbf{r})+C_X\Psi_X(\mathbf{r}) , \tag{22}$$

TABLE VI. Table showing oscillator strengths calculated at various pressures for the transitions EΓ1-HH1 and EX1-HH1 which are shown in Fig. 26 for the (GaAs,68 Å/$Al_{0.28}Ga_{0.72}As$, 68 Å) (001) superlattice.

Hydrostatic pressure (kbar)	Oscillator strength $F_{E\Gamma 1\text{-}HH1}$	Oscillator strength $F_{EX1\text{-}HH1}$
10	5.3	0.0
20	5.1	6.3×10^{-3}
30	3.4	1.2
40	3.2	3.3×10^{-3}

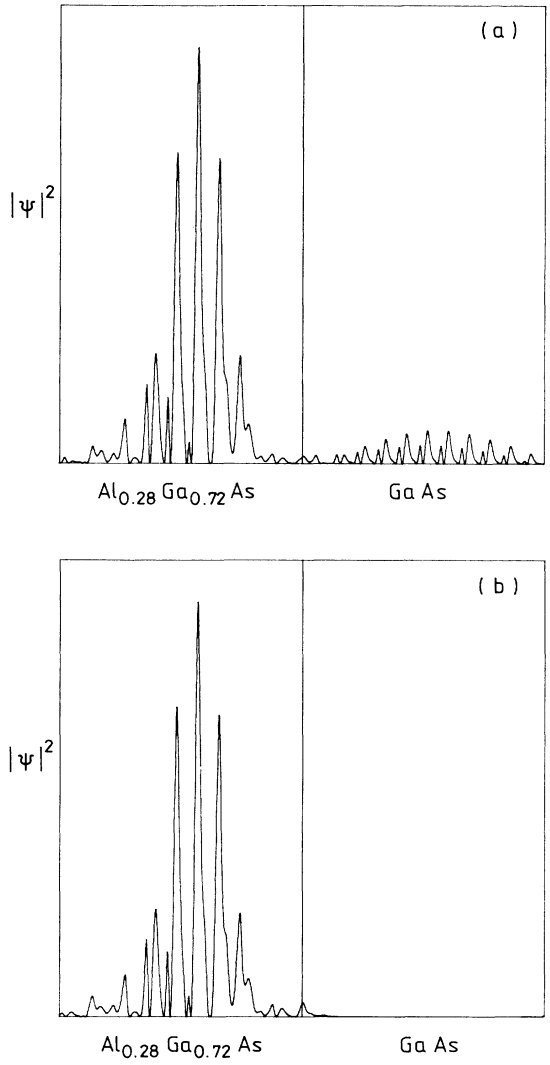

FIG. 27. (a) Charge density of the lower-energy state in the quasidegenerate pair of EX1 states, plotted along the superlattice axis in the [001] direction, at the center of the superlattice Brillouin zone, in the (GaAs,68 Å/$Al_{0.28}Ga_{0.72}As$,68 Å) (001) superlattice at 30 kbar (see Fig. 26). (b) Charge density remaining from (a) after the zone-center components in the wave function have been removed.

which leads to the secular determinant

$$\begin{vmatrix} E_\Gamma - E & V_{\Gamma,X} \\ V_{X,\Gamma} & E_X - E \end{vmatrix} = 0 , \tag{23}$$

where

$$V_{\Gamma,X} \cong \int F_\Gamma(z) F_X(z) dz \int \phi_\Gamma^*(\mathbf{r}) V_{\mathrm{SL}}(\mathbf{r}) \phi_X(\mathbf{r}) d^3\mathbf{r} . \tag{24}$$

In (24), $V_{\mathrm{SL}}(\mathbf{r})$ is the superlattice potential defined in Sec. III B. The eigenvalues of (23) are

$$E = \tfrac{1}{2}(E_\Gamma + E_X \pm \delta) , \tag{25}$$

where

$$\delta = [(E_\Gamma - E_X)^2 + 4 \mid V_{\Gamma,X} \mid^2]^{1/2} . \tag{26}$$

At the crossing, $E_\Gamma = E_X$, and so the repulsion in energy of the mixed states is $\Delta E = 2 \mid V_{\Gamma,X} \mid$ and the wave functions are

$$\Psi(\mathbf{r}) = 1/\sqrt{2}[\Psi_\Gamma(\mathbf{r}) \pm \Psi_X(\mathbf{r})] . \tag{27}$$

The major limitation of this model is that it overestimates the amplitude of the wave functions (27) in the GaAs layers because, in reality, there is more than just one zone-edge-related superlattice state interacting with the zone-center-related state. However, Eq. (24) shows some important features. Let us consider two different situations: one in which F_Γ and F_X are localized in the same layers and the other in which F_Γ and F_X are localized in spatially separated layers. These two situations can be satisfied by changing the band offset (see Fig. 9). For example, with an 85:15 offset, F_X is localized in GaAs whereas for a 71:29 offset it is localized in $Al_xGa_{1-x}As$. In both cases $\mid V_{\Gamma,X} \mid$ will be finite and of the same order of magnitude (see Ref. 4 for Γ-X mixing with an 85:15 offset). When F_Γ and F_X are localized in the same layer, the overlap integral in (24) is of the order of 1 whereas it is $\ll 1$ for the other case. Therefore, in order to obtain finite $\mid V_{\Gamma,X} \mid$, $\phi_X(\mathbf{r})$ must be very different in going from GaAs to $Al_xGa_{1-x}As$. In other words, the Γ-X mixing is controlled essentially by the difference in the periodic part of the zone-edge Bloch states of GaAs and $Al_xGa_{1-x}As$.

VI. CONCLUSIONS

The electronic and optical properties of the superlattices (and MQWS's) which have been described here rest on a delicate balance between dimensional conditions and the microscopic properties of the superlattice potential. The underlying dimensional conditions may be considered to be the periodicity of the superlattice, the relative widths of the constituent layers and the band offsets. The form of the full superlattice potential is also intimately connected with the underlying dimensional conditions but is derived primarily from differences between atomic (pseudo)potentials. The form factors from which the band structure of the host crystal is generated give rise to a set of eigenvalues $E_{n\mathbf{k}s}$ which, within the context of our scheme, can also be regarded as a set of dimensional conditions. The sensitivity of the zone-edge-related states to the $E_{n\mathbf{k}s}$ was discussed. Taken in isolation, these dimensional conditions may be used to give a useful guide to the envelope structures of the states near a particular band edge. However, the finite details (and, in fact, the origin) of the electronic states are controlled by the Fourier components of the superlattice potential at and clustered around the bulk reciprocal lattice vectors. Scattering processes associated with wavelengths which are comparable with the widths of the layers are largely irrelevant in the determination of the electronic and optical properties of the superlattices. The short-wavelength scattering processes also determine the Γ-X mixing which gives rise to observable transitions from HH1 to the zone-edge-related states.

Energy levels, transition energies, optical matrix elements, oscillator strengths and wave functions in real (and momentum) space have been presented in order to describe crossings between zone-center and zone-edge-related superlattice states. In particular, we have used a representative set of measured transition energies under hydrostatic pressure to make a direct comparison with experiment. A good agreement was obtained although small but noticeable uncertainties in the pressure dependence of the indirect exciton energies and the band offsets and in the (bulk) pressure coefficients of the band edges of $Al_xGa_{1-x}As$ prevented us from achieving a truly quantitative agreement. However, a deeper conceptual understanding of the response of superlattice electronic states to changes in alloy composition and hydrostatic pressure has been achieved and will serve as a basis for future studies.

ACKNOWLEDGMENTS

We wish to acknowledge financial support from the Science and Engineering Research Council, United Kingdom (M.A.G. and D.N.) and from the Royal Signals and Radar Establishment at Malvern (M.A.G.). One of us (M.J.) wishes to thank IBM (Yorktown Heights) for their hospitality.

*Present address: British Telecommunications Research Laboratories, Martlesham Heath, Ipswich, Suffolk, IP5 7RE, England, United Kingdom.

[1]R. Dingle, in *Festkorperprobleme,* edited by H. J. Queisser (Vieweg, Braunschweig, 1975), Vol. 15, p. 21.

[2]G. Sai-Halasz, R. Tsu, and L. Esaki, Appl. Phys. Lett. **30**, 651 (1977).

[3]T. Ando, A. B. Fowler, and F. Stern, Rev. Mod. Phys. **54**, 437 (1982), and references therein.

[4]D. Ninno, K. B. Wong, M. A. Gell, and M. Jaros, Phys. Rev. B **32**, 2700 (1985).

[5]D. Ninno, M. A. Gell, and M. Jaros, J. Phys. C **19**, 3845 (1986).

[6]Y. C. Chang and J. N. Shulman, Phys. Rev. B **31**, 2069 (1985).

[7]J. N. Shulman and T. C. McGill, Phys. Rev. B **19**, 6341 (1979).

[8]M. A. Gell, D. Ninno, M. Jaros, and D. C. Herbert, Phys. Rev.

B **34**, 2416 (1986); M. A. Gell and D. C. Herbert (unpublished).
[9]D. J. Wolford, T. F. Keuch, J. A. Bradley, M. A. Gell, D. Ninno, and M. Jaros, J. Vac. Sci. Technol. B **4**, 1043 (1986).
[10]D. Brust and L. Liu, Phys. Rev. **154**, 647 (1967).
[11]F. Bassani and M. Yoshimine, Phys. Rev. **130**, 20 (1963).
[12]S. Bloom and T. K. Bergstresser, Solid State Commun. **6**, 465 (1968).
[13]G. Weisz, Phys. Rev. **149**, 504 (1966).
[14]M. Jaros, Rep. Prog. Phys. **48**, 1091 (1985).
[15]E. Johnson, in *Semiconductors and Semimetals*, edited by R. K. Willardson and A. C. Beer (Academic, New York, 1967).
[16]M. L. Cohen and T. K. Bergstresser, Phys. Rev. **141**, 789 (1966).
[17]H. Neumann, I. Topol, K. R. Schulze, and E. Hess, Phys. Status Solidi **56**, K55 (1973).
[18]E. Hess, I. Topol, K. R. Schulze, H. Neumann, and K. Unger, Phys. Status Solidi **55**, 187 (1973).
[19]A. Baldareschi, E. Hess, K. Maschke, H. Neumann, R. Schulze, and K. Unger, J. Phys. C **10**, 4709 (1977).
[20]F. D. Murnaghan, Proc. Nat. Acad. Sci. **30**, 244 (1944).
[21]H. J. McSkimin, A. Jayaraman, and P. Andreatch, J. Appl. Phys. **38**, 2362 (1967).
[22]D. J. Wolford and J. A. Bradley, Solid State Commun. **53**, 1069 (1985).
[23]K. K. Mon, K. Hess, and J. Dow, J. Vac. Sci. Technol. **19**, 564 (1981).
[24]B. Welber, M. Cardona, C. K. Kim, and S. Rodriguez, Phys. Rev. B **12**, 5729 (1975).
[25]S. Lee, J. Sanchez-Dehesa, and J. D. Dow, Phys. Rev. B **32**, 1152 (1985).
[26]See references in M. Neuberger, *Handbook of Electronic Materials* (Plenum, New York, 1971), Vol. 2.
[27]W. M. Yim, J. Appl. Phys. **42**, 2854 (1971).
[28]A. Onton, Proceedings of the Tenth International Conference on the Physics of Semiconductors, Cambridge, 1970 (unpublished).
[29]A. C. Carter, P. J. Dean, M. S. Skolnick, and R. A. Stradling, J. Phys. C **10**, 5111 (1977).
[30]F. Bassani and G. Pastori Parravicini, *Electronic States and Optical Transitions in Solids* (Pergmon, New York, 1975).
[31]R. Braunstein and E. O. Kane, J. Phys. Chem. Solids **23**, 1423 (1962).
[32]P. Lawaetz, Phys. Rev. B **4**, 3460 (1971).
[33]J. M. Chamberlain and R. A. Stradling, Solid State Commun. **7**, 1275 (1969).
[34]Q. H. F. Vrehen, J. Phys. Chem. Solids **29**, 129 (1968).
[35]N. E. Christensen, Phys. Rev. B **30**, 5753 (1984), and references therein.
[36]G. D. Pitt, J. Lees, R. A. Hoult, and R.A. Stradling, J. Phys. C **6**, 3282 (1973).
[37]D. J. Stukel and R. N. Euwema, Phys. Rev. **188**, 1193 (1969).
[38]G. Bastard, Phys. Rev. B **24**, 5693 (1981).
[39]R. A. Morrow and K. R. Brownstein, Phys. Rev. B **30**, 678 (1984).
[40]S. R. White, G. E. Margues, and L. J. Sham, J. Vac. Sci. Technol. **21**, 544 (1982).
[41]Q. C. Zhu and H. Kroemer, Phys. Rev. B **27**, 3519 (1983).
[42]W. R. Frensley and H. Kroemer, Phys. Rev. B **16**, 2642 (1977).
[43]M. Jaros, K. B. Wong, M. A. Gell, and D. J. Wolfrod, J. Vac. Sci. Technol. B **3**, 1051 (1985).
[44]M. A. Gell, K. B. Wong, D. Ninno, and M. Jaros, J. Phys. C **19**, 3821 (1986).
[45]We use the term "active" to define the layer in which a superlattice state is confined. Since superlattice states can be confined in either the GaAs or the alloy layer, the term active (or barrier) can be ascribed to either of the layers depending on the state in question.
[46]I. Ivanov and J. Pollmann, Solid State Commun. **32**, 869 (1979).
[47]G. B. Bachelet and N. E. Christensen, Phys. Rev. B **31**, 879 (1985).
[48]S. L. Richardson, M. L. Cohen, S. G. Louie, and J. R. Chelikovsky, Phys. Rev. B **33**, 1177 (1986).
[49]W. E. Pickett, S. G. Louie, and M. L. Cohen, Phys. Rev. B **17**, 815 (1978).
[50]J. Ihm, P. K. Lam, and M. L. Cohen, Phys. Rev. B **20**, 4120 (1979).
[51]G. Bastard, E. E. Mendez, L. L. Chang, and L. Esaki, Phys. Rev. B **26**, 1974 (1982).